Sino-Korean–Yangtze suture, Huwan detachment, and Paleozoic–Tertiary exhumation of (ultra)high-pressure rocks in Tongbai–Xinxian–Dabie

Lothar Ratschbacher[1], Leander Franz,
Eva Enkelmann, Raymond Jonckheere, and Axel Pörschke
Geowissenschaften, Technische Universität Bergakademie Freiberg,
D-09599 Freiberg, Germany
Bradley R. Hacker
Geological Sciences, University of California, Santa Barbara, CA 93106, USA
Shuwen Dong, Yueqiao Zhang
Chinese Academy of Geological Sciences, Beijing 100037, P.R. China

ABSTRACT

Three sutures characterize the Qinling–Dabie–Sulu orogen in the Tongbai–Xinxian–Dabie area: the Silurian Sino-Korean Craton–Erlangping intra-oceanic arc suture, the Silurian Erlangping arc–Qinling microcontinent suture, and the Early Triassic Qinling microcontinent–Yangtze Craton suture. Controversy regarding the age of the Sino-Korean Craton–Yangtze Craton collision is resolved by recognizing that there was Paleozoic collision between the Qinling microcontinent and the Sino-Korean Craton and Mesozoic collision between the Qinling microcontinent and the Yangtze Craton. Qinling microcontinent characteristics are ~1.0 Ga orogeny, ~0.8–0.7 Ga arc formation and rifting, and Late Silurian–Early Devonian (~400 Ma) arc magmatism with concomitant metamorphism up to granulite facies (peak: 680–740°C at 0.9–1.1 GPa). A common Proterozoic history links the Qinling microcontinent to the Yangtze Craton; its ~400 Ma arc, its fore-arc basin, and its separation from the Yangtze Craton by the partly oceanic Huwan mélange make the Qinling microcontinent distinct. The Huwan contains elements of the Qinling microcontinent and its arc, the Paleotethyan ocean floor, and possibly the Yangtze Craton. Quartz eclogites (540–590°C, 2.1 GPa) signify ~315 Ma subduction. Devonian to Permian eclogite zircon ages, Late Carboniferous to Early Jurassic $^{40}Ar/^{39}Ar$ and Rb/Sr mineral ages in the fore-arc and its basement, and static,

[1] E-mail: lothar@geo.tu-freiberg.de

Late Permian blueschist metamorphism in the upper plate basement testify to subduction throughout the Late Paleozoic.

The ~10 km wide Huwan detachment bounds the high- and ultrahigh-pressure rocks of the Xinxian–Hong'an block (pressure peak at ≥240 Ma) along their northern margin. Its high-strain deformation describes passage of rocks through the lithosphere by subhorizontal N–S extension and vertical contraction, showcased by condensed Triassic isograds (~420°C, ~0.4 GPa in the hanging wall and ~530°C, 2.2 GPa in the footwall). Triassic crustal exhumation rates were 1.9–1.4 mm/a. Syn-kinematic phengite grew as early as ~235 Ma, and the main retrograde deformation was 224–195 Ma. The Tongbai–Xinxian area shows a massive 130–115 Ma cluster of cooling ages, reflecting regional cooling after granitoid injection and regional Cretaceous heating. Apatite fission-track ages cluster at 80–55 Ma and signify cooling related to transtension that coincides with rifting marked by Late Cretaceous–Eocene red bed deposition throughout eastern China. Exhumation rates of for the last 70 Ma have been ~0.06 mm/a.

INTRODUCTION

The Qinling–Tongbai–Xinxian–Dabie–Sulu orogen stretches for ~2000 km in east-central China (Fig. 1). Controversies exist about the location and number of sutures and the age of collision between the northern Sino-Korean (SKC) and the southern Yangtze Craton (YC). Resolving these controversies is important because the orogen hosts at least two distinct ultrahigh-pressure events (e.g., Yang et al., 2005). Researchers in the Qinling have favored a Paleozoic amalgamation (e.g., Kröner et al., 1993) or a Paleozoic collision overprinted by Mesozoic intracontinental shortening (e.g., Mattauer et al., 1985). In contrast, work in the Dabie–Sulu demonstrated Triassic YC subduction beneath a collage of rock units traditionally attributed to the SKC (e.g., Ames et al., 1996; Hacker et al., 1996, Wallis et al., 1999). In the Qin Mountains ("Qinling"), a clearer picture has emerged (e.g., Ratschbacher et al., 2003 and references therein). There, intra-oceanic arc formation at ~490–470 Ma (the Erlangping–Danfeng–Heihe unit) was followed by accretion of the Qinling microcontinent ("Qinling unit") to the intra-oceanic arc and the SKC and imprint of a ~400 Ma Andean-type magmatic arc onto the Qinling and Erlangping–Danfeng–Heihe units and the SKC. Oceanic subduction continued south of the Qinling unit, producing a Carboniferous high-pressure (HP) mélange belt (Sun et al., 2002), and terminated with the attempted north-directed subduction of the YC (e.g., Hacker et al., 2000). Preservation of ultrahigh-pressure (UHP) minerals, including coesite in eclogites and host paragneisses in Hong'an–Dabie–Sulu, demonstrates subduction of supra-crustal rocks of the YC down to mantle depths (e.g., Zhou et al., 1993; Eide and Liou, 2000 for the Hong'an–Xinxian area).

Most models for exhumation of the Triassic UHP rocks (e.g., Hacker et al., 2000, 2004; Faure et al., 1999, 2003; Webb et al., 1999, 2001) suggest a major role of sub-horizontal extension that apparently followed buoyant rise of the UHP rocks through the mantle. The north-dipping Huwan detachment was identified as the major high-strain, normal-sense shear zone at the top of the strongly deformed HP–UHP rocks in northern Hong'an (this area is called "Xinxian" in the Chinese literature—a usage we follow in this paper; Rowley and Xue, 1996; Webb et al., 1996; Hacker et al., 1998, 2000; Webb et al., 1999, 2001). The Xinxian area has also been suggested to constitute the only portion of the orogen where the northern boundary of the HP–UHP units coincides with the SKC–YC suture (e.g., Hacker et al., 2000, 2004; Ratschbacher et al., 2003; Faure et al., 2001).

Although portions of the UHP rocks were exhumed to the surface by the Jurassic (Grimmer et al., 2003; Wang et al., 2003; Wan et al., 2005), Cretaceous and Cenozoic deformation contributed to exhumation of the present exposure level from mid-crustal depths. The associated structures dominate the orogenic architecture of the Dabie Shan (e.g., Ratschbacher et al., 2000).

SCOPE OF THIS STUDY

Herein we address the following controversies based on new and available geologic, geochronologic, petrologic, and structural data from the Tongbai–Xinxian–northern Dabie area: Where is the suture between SKC and YC? Are there intervening microcontinents? What was the role of the Carboniferous HP metamorphism along the northern edge of the YC? What is the pressure–temperature–time–deformation (PTtd) history of the Huwan detachment shear–fault zone during the Triassic orogeny? What is the PTtd history of the Proterozoic–Paleozoic units north of well-documented Triassic HP–UHP orogen that are ascribed to the SKC? How was the collision zone overprinted in the Cretaceous–Tertiary? Our study highlights the differences between the HP–UHP orogen and its northern foreland, shows that the foreland units are part of the Qinling microcontinent, and provides a comprehensive tectonic scenario for the SKC–YC suture zone from the Paleozoic to Recent.

GEOLOGIC UNITS OF THE NORTHERN TONGBAI–XINXIAN–DABIE

The northern Tongbai–Xinxian–Dabie region is underlain by a number of fault-bounded units that are correlated with similar—often more complete—units in the Qinling farther west (e.g., Ratschbacher et al., 2003). These units are described below from north to south. Figures 2 and 3 summarize geologic and geochronologic data substantiating this subdivision.

Sino-Korean Craton and Kuanping Unit

The basement of the SKC comprises the 2.6–2.0 Ga Taihua gneiss and the Xiong'er Group (e.g., Kröner et al., 1988). The Kuanping unit, chiefly amphibolite- to greenschist-facies marbles and two-mica quartz schists, was interpreted as overlying passive margin sedimentary rocks or an accretionary wedge (see e.g., Ratschbacher et al., 2003). Two $^{40}Ar/^{39}Ar$ ages (434 ± 2 Ma for metamorphic hornblende and 433 ± 2 Ma for magmatic hornblende in diorite of the Huanggang intrusive complex; Zhai et al., 1998) likely typify the Silurian–Devonian arc that overprints the Kuanping, Erlangping, and Qinling units (see below; Ratschbacher et al., 2003).

Erlangping Unit

The Erlangping Unit consists of greenschist- to amphibolite-facies volcanic and plutonic rocks, fine-grained clastic rocks, and chert with Cambrian–Silurian fossils (e.g., Niu et al., 1993); geochemical data suggest it is an Early Ordovician (~470–490 Ma) intra-oceanic arc (e.g., Xue et al., 1996a). In Tongbai and Xinxian, one ~485 Ma K/Ar age of unknown type (R.G.S. Henan, 1989) may date this complex; a 404 ± 5 Ma $^{40}Ar/^{39}Ar$ hornblende age from amphibolite (Zhai et al., 1998) and a ~407 Ma K/Ar age (again of unknown type, R.G.S. Henan, 1989) are likely associated with the Silurian–Devonian arc (see below).

Qinling Unit

In the Qin Mountains, the Qinling unit includes a variety of rocks and its internal structure is not well understood (e.g., Ratschbacher et al., 2003). The structurally lower Qinling includes biotite–plagioclase gneisses, amphibolites, calc-silicate rocks, garnet–sillimanite gneiss, and marble (Xue et al., 1996a); the upper Qinling consists of marble with minor amphibolite and garnet–sillimanite gneiss (You et al., 1993). In Tongbai–Xinxian, the Qinling unit has been subdivided into several units, whose relationships are controversial. Our field survey results generally correspond with the subdivision proposed by Li S.-G. et al. (1995, 2001). In northwestern Tongbai, marble overlies felsic orthogneiss with granulitic enclaves and xenoliths derived from mafic igneous and sedimentary protolith; zircon $^{207}Pb/^{206}Pb$ evaporation ages are 470 ± 20 Ma and 470 ± 14 Ma for the protoliths of two-pyroxene granulites (~800°C and 1.0 GPa) and 435 ± 14 Ma for the enclosing granodioritic gneiss (Kröner et al., 1993). Metaquartzite and metasedimentary garnet granulite gave detrital zircon ages of 2555 ± 8 Ma and 827 ± 10 Ma, respectively. Okay et al. (1993) interpreted the orthogneiss as retrograde granulite and the marble as intercalations in the granulite–gneiss sequence. Here, we suggest that the mafic granulites are part of the intra-oceanic arc sequence of the Erlangping–Danfeng–Heihe unit, that the metasedimentary rocks are associated clastics, and that the enclosing orthogneiss likely belongs to the Silurian–Devonian arc, whose “regional contact metamorphism” is dated by a 404 ± 2 Ma $^{40}Ar/^{39}Ar$ hornblende age (form a felsic garnet–two-pyroxene granulite; Zhai et al., 1998).

The greenschist- to amphibolite-facies Guishan complex (the lower part of the Xinyang “Group” of the Chinese literature) consists of gneiss, amphibolite, garnet–mica schist, chlorite–albite schist, marble, and quartzite; the protoliths of some of these rocks were interpreted as metavolcanic: keratophyre, andesitic tuff, and basalt (e.g., Xu et al. 1992). This unit reappears south of the Nanwan “Formation” (the upper part of the Xinyang Group) as the Dingyuan complex (e.g., Suo et al., 1993; Li et al., 2001), suggesting that the overall structure of the Qinling unit in Xinxian is a synform. The Guishan complex yielded a 392 ± 25 Ma U/Pb zircon age for felsic metavolcanic rock in its upper part (Ye et al., 1994; see also Figure 3b for a summary of important Qinling geochronology in Xinxian), $^{40}Ar/^{39}Ar$ hornblende ages of 401 ± 4 Ma (garnet amphibolite; Niu et al., 1994), 316 ± 1 Ma (amphibolite), and 304 ± 10 Ma (amphibolite of uncertain affinity, perhaps part of the Danfeng unit, Zhai et al., 1998), a 254 ± 1 Ma $^{40}Ar/^{39}Ar$ muscovite age (Xu et al., 2000), and two $^{40}Ar/^{39}Ar$ K-feldspar ages of 225 ± 6 Ma (Niu et al., 1994) and ~240 Ma (this study). Zircons from quartzofeldspathic gneiss with mafic layers at the very southern edge of the Dingyuan complex range from 739 Ma and 638 Ma (n=10, peaks at 729 ± 15 and 659 ± 19 Ma, U/Pb SHRIMP, Hacker et al., 2000). The Sujiahe gabbro at the northern edge of the Dingyuan complex yielded 639–440 Ma zircon ages with a weighted mean of 22 spots at 582 ± 11 Ma (U/Pb SHRIMP; Liu et al., 2004a). Rb/Sr whole-rock isochrons yielded 391 ± 13 and 444 ± 31 Ma (Ye et al., 1994 and Li et al., 2001, respectively). A Sm/Nd whole-rock isochron gave 446 ± 23 Ma on greenschist-facies volcanic rocks; major and trace element geochemistry indicates that these rocks formed in a magmatic arc (Li et al., 2001). The Dingyuan complex had yielded $^{40}Ar/^{39}Ar$ phengite cooling ages of 241 ± 2 Ma from granite mylonite (Liu et al., 2004a; Balifan unit; sample location unclear), and 234 ± 2 Ma from mylonitic quartzofeldspathic schist (Webb et al., 1999).

The Luzhenguan complex in northern Dabie is correlated with the Guishan complex on the basis of lithology, and consists of a lower unit of metavolcaniclastic rocks, granitoid, and gneiss, and an upper quartz–mica schist; it is unclear whether nearby quartzite, phyllite, and marble belong to the Luzhenguan or the overlying Foziling unit (see below, Li et al., 2001, Chen et al., 2003). Six granites yielded U/Pb zircon ages of 766–719 Ma, one quartzite has single-grain detrital zircon age components of ~0.75, ~1.5, and ~1.9 Ga (Pb/Pb evaporation; Chen et al., 2003), and one garnet–biotite schist gave ages ranging from 735 to 660 Ma (U/Pb SHRIMP, Hacker et al., 2000). Granodiorite and dioritic gneiss yielded $^{40}Ar/^{39}Ar$ hornblende ages of 742 ± 5 and 770 ± 10 Ma, and micaschist and garnet–biotite schist gave $^{40}Ar/^{39}Ar$ muscovite ages of ~242 and ~218 Ma, and ~180 Ma for K-feldspar from a deformed granitic dike (Hacker et al., 2000).

The Nanwan unit contains greenschist-grade turbiditic slate, phyllite, quartz micaschist, and quartzite. Its equivalent in northern Dabie, the Foziling "Group", comprises greenschist- to amphibolite-facies, monotonous, mostly fine-grained, well-bedded siltstone and shale, minor volcanic rock, with a local basal quartzite and marble (e.g., Chen et al. 2003); the Foziling Group is thrust onto Carboniferous sandstone, siltstone, and shale (e.g., Okay et al., 1993). The Nanwan and Foziling units have variably been interpreted as YC passive margin, SKC fore-arc flysch, SKC back-arc flysch, or accretionary wedge (see Li et al., 2001 for discussion). Li et al. (2001) used Nd model ages and $\varepsilon_{Nd}(0)$ values to suggest that the Foziling rocks originated within an active continental margin along the SKC (equivalent to the Silurian–Devonian arc in this paper). Carboniferous coals with intercalated marine shales locally overlie these units. Here, we interpret the Nanwan and Foziling units as fore-arc basin sediments, deposited on the Guishan–Dingyuan–Luzhenguan complexes that received detritus from these units, the Silurian–Devonian arc, and its Proterozoic basement (see below). This interpretation is supported by detrital zircons from Foziling quartzites that yielded age groups of 2.5, 1.9, 1.5, 0.8, and 0.4 Ga (Chen et al., 2003). The Foziling unit has given muscovite and biotite K/Ar ages from 225 to 204 Ma (Chen et al., 1993), and $^{40}Ar/^{39}Ar$ muscovite ages of ~271 Ma (this study), ~264 Ma and ~261 Ma (Niu et al., 1994). Several Devonian conglomerate localities along the Shang–Dan fault (i.e. along the northern margin of the Liuling unit—the likely equivalent of the Nanwan unit in Qinling) are associated with turbidites and pyroclastic sediments derived from the Qinling unit, an “ophiolitic assemblage”, and mafic volcanic rocks; Yu and Meng (1995) suggested a fore-arc origin for these rocks. The fossiliferous Upper Devonian siliciclastic rocks are conformably overlain by a sequence of shallow-marine carbonates, turbidites, debris flow deposits, and “slumps”, and a shallowing upward sequence of proven Lower Carboniferous and suspected Carboniferous to Permian age (Yu and Meng, 1995). Metaconglomerate near Danfeng, in the northernmost Liuling unit, gave detrital zircon ages of ~1.0 Ga (n=3), 782 ± 11 Ma (n=3), and 403 ± 7 Ma (three probably metamorphic overgrowths), indicating sources within the Qinling unit and the Silurian–Devonian arc (U/Pb SHRIMP, Ratschbacher et al., 2003).

Silurian–Devonian magmatic arc

Within the Qin Mountains, a suite of relatively undeformed Late Silurian–Early Devonian plutons intrude the SKC, the Kuanping, Erlangping–Danfeng–Heihe, and Qinling units; U/Pb zircon, Sm/Nd and Rb/Sr whole-rock, and $^{40}Ar/^{39}Ar$ hornblende ages from these plutons and associated regional metamorphism cluster at ~404 Ma (n=25; Figure 3a). This magmatic–metamorphic event was interpreted as an Andean-style continental margin arc facing a subduction zone located south of the Qinling unit (e.g., Ratschbacher et al., 2003).

Huwan “mélange”

Field mapping, geochronology, and locally distinctive lithology allow delineation of a separate unit between the Qinling unit in the north and the YC in the south (compare also Li et al., 2001; Ye et al., 1993, 1994). Definition of this unit has been hindered by strong deformation within a ~5–10 km wide zone straddling the southern part of the Qinling unit and the northern part of the HP–UHP units in southern Xinxian (the northern Dabie–Xinxian complex, see below); here we attribute this deformation mostly to the Triassic Huwan shear zone (see below). Confusion arises because this unit has been assigned to various complexes. For example, the Xinyang Group has been divided in Xinxian into the northern Nanwan “flysch” and the southern Balifan “tectonic mélange” (Zhong et al., 1999; 2001; Xu et al., 2000; Sun et al., 2002; Liu et al., 2004 a,b), which likely corresponds to the Sujiahe “mélange” of Jian et al. (1997). In the Chinese literature, the Huwan mélange has also been named the eclogite-bearing Huwan “formation” and was considered to be the southern part of the Sujiahe “Group”, whose northern part is the Dingyuan “formation” (see above). These ambiguities in the definition of units have hindered the assignment of dated rocks. For example, whereas Jian et al. (1997) define their Xiongdian eclogite as part of the Sujiahe mélange, Sun et al. (2002) classified their Xiongdian eclogite body as part of the Huwan "shear zone".

The Huwan mélange contains partly mylonitized, elongated blocks of eclogite, gabbro, (epidote-) amphibolite, marble, and quartzite; augen gneiss, quartzofeldspathic schist and graphitic schist may form an argillic matrix to these blocks. Both blocks and matrix have been subjected to greenschist- to amphibolite-facies metamorphism. The marbles contain Ordovician fossils (Ye et al., 1994). Where defined, the boundaries of the Huwan mélange are north-dipping deformation zones. The "Balifan–Sujiahe" eclogites yielded peak metamorphic conditions of 600–730°C and 1.4–1.9 GPa and retrograde metamorphism at 530–685°C and ~6 kbar according to Fu et al. (2002), and 550–570°C and ~2.1 GPa according to Liu et al. (2004b); the latter values correspond to our own PT estimates (540–600°C and 2.0 GPa, see below). An enriched LREE signature and $\varepsilon_{Nd}(t)$ values of –1.9 to 5.8 indicate oceanic basalts as protoliths; these characteristics distinguish these eclogites clearly from the YC eclogites of Xinxian–Hong'an–Dabie (northern Dabie–Xinxian unit, see below; Fu et al., 2002).

The Xiongdian quartz-eclogite bodies have seen four independent U/Pb zircon studies (Fig. 3c). Jian et al. (1997) obtained four concordant fractions; three yielded ages between 400 and 373 Ma, the fourth 300 ± 2 Ma. Jian et al. (2001) interpreted a 424 ± 5 Ma SHRIMP core age as the age of the protolith and a 301 ± 13 Ma rim age as the age of HP metamorphism; ages of 408–335 Ma were taken as mixed. Sun et al. (2002) studied two different bodies: Zircon cores from eclogite 99XD-1 gave a range of spot ages (SHRIMP, n=5) of which 398 ± 5 Ma is likely the protolith age; a second group of core ages at 324 ± 4 Ma (n=8) has unclear meaning. Zircon overgrowths with garnet–omphacite–phengite inclusions have peaks at 323 ± 7 Ma (n=2) and 312 ± 5 Ma (n=11), likely dating the HP metamorphism. Eclogite 99XD-2 yielded core ages between 450 and 350 Ma, with peaks at 433 ± 9 and 367 ± 10 Ma that were interpreted as the protolith age; two other core and overgrowth groups likely formed during HP metamorphism and retrograde metamorphism outside the garnet stability field at 316 ± 8 and 307 ± 4 Ma, respectively. Gao et al. (2002) found SHRIMP zircon spot ages of 449 ± 14 and 307 ± 14 Ma, and a 216 ± 4 Ma (n=6) cluster in their Xiongdian eclogite. Finally, one of the eclogite bodies gave a Sm/Nd garnet–whole-rock isochron of 422 ± 67 Ma, a Rb/Sr whole-rock age of 404 ± 34 Ma, and a $^{40}Ar/^{39}Ar$ barroisite age of 399 ± 1 Ma (Ye et al., 1993). Webb et al. (1999) reported a geologically questionable 310 ± 3 Ma $^{40}Ar/^{39}Ar$ phengite age from their Xiongdian eclogite and a 233 ± 2 Ma phengite age in a top-N shear band in the enclosing quartzofeldspathic gneiss and micaschist; the Triassic overprint is supported by a muscovite $^{40}Ar/^{39}Ar$ age of ~243 Ma from the "Xiongdian rock formation" (Ye et al., 1994). Major-, trace-element and isotope geochemistry indicate little crustal contamination for the basaltic andesite and basaltic protoliths of the Xiongdian eclogites (Li et al., 2001). Most likely, the Xiongdian eclogites represent Middle Silurian–Early Devonian mafic volcanic rocks that were subducted in the Late Carboniferous and overprinted in the Triassic during the subduction of the leading edge of the YC (see below).

The Hujiawan eclogite crops out northwest of the Xiongdian bodies and yielded a SHRIMP zircon age of 311 ± 17 Ma without inherited components (Sun et al., 2002). Conventional U/Pb zircon geochronology gave concordant ages of 631 ± 3 Ma (one fraction; likely the protolith age), 533 ± 23 Ma (one fraction), 377 ± 7 Ma (two fractions interpreted as "mixed ages"), and ~300 Ma (HP metamorphism); the trace-element and isotopic characteristics, suggesting an island-arc basalt, differ from the Xiongdian bodies (Li et al., 2001).

The Qianjinhepeng eclogite (>1.2 GPa, 610 ± 40°C) is embedded in quartzofeldspathic gneiss at the northern rim of the Huwan mélange. It gave zircon SHRIMP ages of 933 ± 25 Ma (one core), a cluster of 716 ± 28 Ma (n=4), likely the protolith age, and a 534–229 Ma range of spot ages (8 spots between 315 ± 17 and 229 ± 12 Ma); the youngest age was interpreted as the maximum age of the HP metamorphism (Liu et al., 2004a).

The Huwan mélange has yielded Permo–Triassic cooling ages: $^{40}Ar/^{39}Ar$ muscovite ages of ~267 Ma, ~226 Ma (Niu et al., 1994), ~263 Ma (Xu et al., 2000), ~243 Ma , ~230 Ma (Ye et al., 1993), and ~206 Ma (Webb et al., 1999). Four Rb/Sr muscovite–plagioclase–whole-rock isochrons of 259 ± 33, 236 ± 11, 230 ± 40, and 225 ± 8 Ma of unspecified mylonitic rocks likely date deformation related to the Huwan shear zone (see below, Ye et al., 1993).

Northern Dabie–Xinxian complex (HP–UHP metamorphic Yangtze Craton)

The Northern Dabie–Xinxian complex, also called the Xinxian "Formation" in the Chinese literature, consists of granitic to granodioritic gneiss and supracrustal rock that experienced proven HP–UHP conditions. Pressures apparently decrease both northward and southward within this unit (Zhang and Liou, 1994; Cui and Wang, 1995). Liu et al. (2004b) quantified the PT conditions of eclogites within the northern HP (quartz-eclogite) zone and southern UHP (coesite-eclogite) zone at 470–500°C, 1.4–1.7 GPa and 620–670°C, 2.6–2.9

GPa, respectively; we obtained ~530°C and 2.2 Ga for an eclogite from the quartz-eclogite zone (see below).

Sun et al. (2002) obtained a protolith age of 752 ± 17 Ma and a 232 ± 10 Ma age for the HP Xuanhuadian quartz eclogite (SHRIMP U/Pb zircon; Fig. 2b; see also Fig. 3d for a summary of important northern Dabie–Xinxian geochronology). The Huwan eclogite (Fig. 2b; 570 ± 30°C, >1.2 GPa), grouped into the southern part of the "Huwan HP unit" by Liu et al. (2004a), gave a concordant zircon SHRIMP age of 733 ± 10 Ma (n=20), likely its protolith age. From its location, lithological association, and the lack of a Paleozoic age component, we suggest that this eclogite is part of the northern Dabie–Xinxian complex. The Tianpu coesite–eclogite (Fig. 2b, 640 ± 30°C, 2.9 ± 0.3 GPa), embedded in granitic gneiss, contains only metamorphic zircons that cluster at 213 ± 5 Ma (n=13); as its phengite Rb/Sr age is 212 ± 7 Ma, these ages are best interpreted as dating post-UHP recrystallization (Liu et al., 2004a). In northern Dabie (the northern part of the Northern Orthogneiss Unit of Hacker et al., 1996), pre-Cretaceous ages of gneisses are 757 ± 1 Ma (Xue et al., 1997) and 707 ± 42 Ma (Xie et al., 2001). Ultramafic and mafic bodies distributed along the northern margin of Dabie also yielded Triassic ages (Hacker et al., 1998; Jahn et al., 1999; Ratschbacher et al., 2000; see summaries in Fig. 2a and in Liu et al., 2001) interpreted as dating its HP–UHP conditions (e.g., Liu et al., 2000, 2001; Xie et al., 2004).

^{40}Ar/^{39}Ar phengite ages from the northern margin of the northern Dabie–Xinxian complex in Xinxian are: 187 ± 1 Ma (granitic gneiss; Xu et al., 2000), 235 ± 2 Ma (felsic gneiss) and 215 ± 1 Ma (micaschist–orthogneiss intercalation; this study). ^{40}Ar/^{39}Ar phengite ages from within the northern Dabie–Xinxian complex are 243 ± 6 Ma (shear band in eclogite), 212 ± 2 Ma (retrograde epidote–actinolite schist), 231 ± 2 Ma (eclogite rim), 224 ± 2 Ma (shear band in gneiss), 222 ± 2 Ma (mylonitized eclogite), 196 ± 2 Ma (host paragneiss to the previous sample; Webb et al., 1999), and 195 ± 1 Ma (gneiss; Eide et al. 1994).

Cretaceous magmatism and related regional metamorphism

In contrast to northern Dabie, no well-documented U/Pb zircon ages are available from the Mesozoic granitoids of Xinxian (Fig. 2). The oldest group of ^{40}Ar/^{39}Ar ages in Xinxian, 130–125 Ma, (Fig 3e; 125–130 Ma; compiled from Niu et al., 1994; Webb et al., 1999; Ratschbacher et al., 2000) overlaps the crystallization ages of Early Cretaceous plutons in the Northern Orthogneiss unit of the northern Dabie Shan and thus likely reflect post-emplacement cooling. Cooling at ~120 Ma in northern Dabie is structurally controlled (Ratschbacher et al., 2000) and this same age is dominant in Xinxian (Fig. 3e). K-feldspar ages from Xinxian overlap the ~100–90 Ma reheating and subsequent cooling documented in Dabie (Ratschbacher et al, 2000).

NEW ^{40}AR/^{39}AR AND FISSION-TRACK GEOCHRONOLOGY

^{40}Ar/^{39}Ar geochronology

We measured ^{40}Ar/^{39}Ar ages on eight mineral concentrates (Fig. 4, Table 1). Analyses were performed at Stanford University and the University of Vienna following analytical procedures of Hacker et al. (1996) and Frimmel and Frank (1998). Four K-feldspars were degassed following the heating schedule adopted for multiple-diffusion domain analysis (Lovera et al., 1997); we refrained, however, from a quantitative evaluation because multiple isothermal, low-T steps identified significant Cl-correlated excess ^{40}Ar (Harrison et al., 1994) and the age spectra are not composed of monotonically increasing steps. Ratschbacher et al. (2003; their Appendix A) outlined adjustments allowing modeling and interpretation of parts of such spectra (e.g., D222d), but in this study the quantitative evaluation does not yield information beyond the qualitative interpretation.

K-feldspar samples D222d and D527b are from the southern Guishan complex. At station D222, the active Jinzhai fault (Ratschbacher et al., 2000) overprints mylonitic rocks. A disturbed hornblende spectrum (deformed amphibolite; Ratschbacher et al., 2003) from this locality and two poorly located muscovite K/Ar ages (Chen et al., 1993) indicate a tectonometamorphic event at <497 and ~450–433 Ma, respectively. The K-feldspar records a regional thermal overprint at ~100 Ma, likely induced by a Cretaceous pluton to the south that shows initial cooling through ~250°C at ~128 Ma and reheating and cooling at 90 ± 10 Ma (Ratschbacher et al., 2000). K-feldspar from a retrogressed, partly mylonitic amphibolite and tourmaline–hornblende gneiss with K-feldspar augen at station D527 suggests mylonitization at >270 Ma and reheating at ~240 Ma. Niu et al.'s (1994) K-feldspar age of ~255 Ma supports a Permo–Triassic low-T overprint in this area; these data also constrain the age of the blueschist-grade overprint in these rocks (see below). Two hornblende ages at ~401 Ma (near D527, Niu et al., 1994) and ~316 Ma (Zhao et al., 1998) suggest a late Paleozoic age for the mylonitization. Sample D337a, from the southernmost margin of the Dingyuan complex, documents reheating and subsequent cooling of Neoproterozoic basement (Hacker et al., 2000; see above) by Cretaceous regional metamorphism at ~125–110 Ma; the pluton east of this station cooled through ~300°C at ~120 Ma (Webb et al., 1999). K-feldspar ages of samples D236 and D329b document the regional Cretaceous (~100–105 Ma) reheating of the HP–UHP Xinxian–Hong'an area, in line with the data of Webb et al. (1999).

Two white-mica ages characterize cooling accompanying deformation within the Huwan shear zone along the northern margin of the Xinxian complex. D538d phengite, from mylonitic but weakly retrogressed gneiss containing numerous shear bands, dates early top-N flow at ~235 Ma; Liu et al. (2004b) obtained phengite Si values of 3.33 atoms per formula unit (p.f.u.) in shear bands in eclogite HW01, likely at our station D538. D539c phengite (core and rim Si values of 3.48 and 3.28 p.f.u) dates top-N flow along phengite-rich shear bands within the retrograde outer margin of a small eclogite body at ~215 Ma, demonstrating a Late Triassic age for late-stage deformation in the Huwan shear zone. White mica in two-mica, gneissic, likely volcaniclastic quartzite D545c yielded ~271 Ma, in line with two other Permian white-mica ages (Niu et al., 1994) from the Foziling unit in Dabie.

Apatite and titanite fission-track geochronology

Twenty-eight samples from metamorphic and magmatic rocks from the northern Dabie and Hong'an–Xinxian areas were selected for apatite (AFT, n=22) and titanite fission-track geochronology (TFT, n=6). See Grimmer et al. (2002) for the methodological and technical aspects of AFT, including the calculation and comparison of ages obtained by the independent ϕ-method and the standard based Z and ζ methods, the evaluation of the Durango, Fish Canyon, and Mt. Dromedary standards, and our approach to T[t]-path modeling. We use ϕ ages. Table 2 lists the sample locations, the AFT dating parameters, and ages; Table 3 gives track-length parameters. Titanite was separated conventionally, mounted in epoxy, ground, and polished with 6.0, 3.0, 1.0, and 0.3 μm diamond suspensions. The mounts were etched for 24 hours in 0.4% HF at room temperature (Jonckheere and Wagner, 2000; Enkelmann et al., 2005), covered with muscovite external detectors, and irradiated in the course of two irradiations in the Thetis reactor at the Institute for Nuclear Sciences of the University at Gent. The muscovite external detectors were etched in 40% HF for 30 minutes at room temperature. Three mounts of Fish Canyon and Mount Dromedary age standards and four mounts of standard uranium glass (CN-5) were included in each irradiation to calculate the ζ-calibration factor (423 ± 25 a cm^2). Track counting was performed on clear titanite surfaces with homogeneous track densities at a nominal magnification of 1000 using a Zeiss Axioplan microscope equipped with the Autoscan system (Autoscan Systems Pty. Ltd.). All suitable grains were counted in samples that contained fewer than 20 grains. Table 4 lists the TFT sample locations, dating parameters, and ages.

Figure 5 combines the regional fission-track age distribution with an interpretation of Cretaceous (Fig. 5a) and Cenozoic structures (Fig. 5b) in Hong'an–Xinxian and northern Dabie (Fig. 5c); the structural interpretation updates that given by Ratschbacher et al. (2000). The AFT ages are Early Cretaceous to late Eocene (145–40 Ma). The subdued topography of the Hong'an–Xinxian area (in general our samples span <200 m elevation difference; Table 2) inhibits any age–altitude correlation. Figure 5 also presents T[t]-path modeling results (using AFTSolve 1.1.3, Ketcham et al., 2000) of samples with a large number of confined tracks. TFT ages are included in the diagrams, but were not used in the modeling. Because there are only weak geologic constraints on the cooling history of the Hong'an–Xinxian area, we set pairs of initial and final constraints. Two closely spaced initial constraints allow the thermal histories to start with cooling or heating; the two final constraints allow the model to find a thermal event that reduces all accumulated tracks and thus accounts for track shortening at ambient temperatures over geological times. Low temperature track-length reduction has been described for fossil tracks in age standards and borehole samples; this reduction is not incorporated into the annealing equations derived from high temperature and short term laboratory annealing experiments on induced fission tracks, which only account for annealing that takes part within the partial annealing zone (see discussion in Jonckheere, 2003a, b).

We obtained similar, slow cooling paths throughout the study area, although we varied the initial constraints over a wide age range (Fig. 5). Assuming a geothermal gradient of 25°C/km, the exhumation rate has been ~0.06 mm/a for the last 70 Ma (the average AFT age of Hong'an–Xinxian; Fig. 3f). Combining the TFT and AFT ages and assuming titanite and apatite closure temperatures of 300°C and 100°C, respectively, gives a slow Late Cretaceous cooling of 5–7°C/Ma for Xinxian and 3–4.5°C/Ma for the northern part of the Northern Orthogneiss unit of Dabie; the relatively high assumed titanite closure temperature is supported by equivalent $^{40}Ar/^{39}Ar$ biotite and TFT ages for 4 of our 6 samples. The apatite confined track-length distributions are typically negatively skewed, broad, and unimodal. In line with the T[t]-path modeling results, this indicates continuous cooling through the ~100°C isotherm to surface temperatures since the time given by the apparent fission-track ages.

Projecting all available AFT ages on a NW–SE section across Hong'an–Xinxian (Fig. 5a, inset) does not show age clusters and, with the possible exception of the Tongbai fault zone (a Late Cretaceous–Early Tertiary strike-slip zone that was reactivated in the Late Cenozoic; Webb et al., 1999; Ratschbacher et al., 2000), no unambiguous correlation with structures.

The same indistinct picture (a large age range over small elevation difference) holds for the northern Dabie Shan, again suggesting slow exhumation rates.

Figure 3f plots all well-documented AFT ages from Tongbai–Hong'an–Xinxian–Dabie area and the northern, eastern and southern forelands of the Dabie Shan (Grimmer et al., 2002; Reiners et al., 2003; Zhou et al., 2003; Xu et al., 2005). Two distinct maxima at 80–55 Ma and ~45 Ma contrast with a broad age range that spans the Cretaceous. These clusters may have significance at a smaller scale: Eocene ages occur mostly along the Tanlu fault in eastern Dabie, where the footwall Dabie block is juxtaposed against the Qianshan basin and, more rarely, in Tongbai–Xinxian. All areas show Late Cretaceous–Tertiary ages.

NEW PETROLOGY

We investigated ~100 samples from the main geological units of the Xinxian area with optical microscopy and selected nine samples for electron-probe microanalysis. We operated the five-spectrometer JEOL JXA-8900R electron microprobe at Freiberg at 15 kV accelerating voltage, 20 nA beam current, and counting times of 20 s for Si, Al, Mg, Ca, Sr, Ba and K, and 30 s for Fe, Ni, Na, Cr, Mn and Ti. Smithsonian Institute and MAC™ standards were used. For the estimate of the peak metamorphic conditions in eclogite, garnet analyses with the highest Mg# (i.e. rim sections) were chosen. Furthermore, paragenetic omphacite with the highest jadeite content and phengite with the highest Si-content were selected for the thermobarometric calculations (cf. Waters and Martin, 1993; Schmid et al., 2000). Peak metamorphic conditions in the other metabasites were calculated using amphibole with the highest Al- and Ti-contents (mostly core analyses) and the associated equilibrium paragenesis. For the thermobarometric modeling of the retrograde PT-path, contact paragenetic metamorphic minerals in retrogressed sections or rim sections of zoned minerals were chosen. Table 5 lists sample locations and parageneses, and summarizes our PT estimates; Figure 6 depicts the PT arrays derived from mineral assemblages and thermobarometry. Tables 6–11 provide microprobe analyses of representative minerals; they are available at http://www.geol.tu-freiberg.de/tectono/E_Links.htm. Mineral abbreviations following Kretz (1983).

Northern Dabie–Xinxian complex

Massive eclogite sample 98196 (station D539) shows the primary mineral assemblage Grt + Omp + Phn + Czo + Qtz, with atoll-shaped garnet porphyroblasts and a weak alignment of the prismatic minerals. There is no petrographic indication for the former stability of coesite in the matrix or as inclusions. Along grain boundaries and cleavages, omphacite is altered to a felted mass of sheet silicates and amphibole. Garnet rims are overgrown by bluish-green amphibole and plagioclase. Other secondary minerals include biotite, formed at the expense of phengite, and titanite that mantles rutile. *Garnet* shows rimward decreasing Mn and Ca and a concomitant increase in Fe and Mg. Typical core and rim compositions are $Alm_{50}Grs_{35}Prp_{3}Sps_{12}$ and $Alm_{63}Grs_{25}Prp_{11}Sps_{1}$, respectively. The bell-shaped Mn profile probably developed during growth under greenschist- to amphibolite-facies conditions (cf. Spear, 1993), and increasing Mg# indicates heating during growth. *Omphacite* has jadeite contents of 28–44 mol% with variable and irregular zoning. *Phengite* is zoned with outward decreasing Si contents of 3.48 –3.28 atoms p.f.u. and decreasing X_{Mg}, highlighting Mg-tschermaks exchange. *Clinozoisite* is unzoned with pistacite contents of ~12 mol%. Secondary *clinoamphibole*, growing at the rims of garnet porphyroblasts, is barroisite and magnesiokatophorite. Secondary *plagioclase* is albite with $An_{<01}$.

A PT estimate for eclogite 98196 is difficult due to the distinct retrograde overprint. Phengite in paragenesis with garnet and omphacite allows an estimate of the peak pressure conditions based on the barometer of Waters and Martin (1993, updated 1996; activity models in Appendix). Garnet compositions yielding the highest activity factor $a^2_{Grs}a_{Prp}$, phengite with the highest Si content, and omphacite with the highest jadeite component were considered to reflect maximum pressure conditions. In sample 98196, the highest $a^2_{Grs}a_{Prp}$ point and the highest Mg# are at the rim, indicating coincidence of peak temperatures and pressures at 2.1–2.2 GPa and 500–550°C. Precise temperature estimates in eclogites, mainly based on Fe–Mg exchange between garnet and omphacite or garnet and phengite (e.g., Krogh, 2000; Green and Hellmann, 1982), are problematic due to our inability to estimate Fe^{3+} in phengite and omphacite (e.g., Schliestedt 1980; Carswell et al. 1997). For omphacite, Fe^{3+} estimates based on charge balance or Na content (e.g., Ryburn et al., 1976; Droop, 1987; Cawthorn and Collerson, 1974) are highly variable and depend critically upon the accuracy of the microprobe analyses. We assumed 50% Fe^{3+}, as recommended by Carswell et al. (2000) and as measured for Dabie eclogites using wet chemistry and XANES (Schmid et al., 2003); this gave 485–535°C for the omphacites with the highest jadeite contents. Due to the small amount of Fe in phengite, methods to determine its ferric iron content often fail (e.g., Schliestedt, 1980). Assuming that ferrous iron equals total iron for garnet and white mica, thermometers provide maximum values; application of Green and Hellman's (1982) garnet–phengite thermometer yielded ~580°C at 2.2 GPa, in accord with Liu et al.'s (2004b) eclogite data for this area. These PT estimates (Fig. 6a) correspond within error to those from coeval quartz eclogites of the southern Dabie Shan (e.g., Okay et al., 1993; Liou et al., 1996; Franz et al., 2001); they also match estimates for the Paleozoic Xiongdian eclogites (see below and Fu et al., 2002).

The metamorphism of eclogites and gneissic country rocks in the Northern Dabie–Xinxian complex is exclusively Triassic–Jurassic (see above). The 232 ± 10 Ma zircon age of the pristine Xuanhuadian eclogite is identical to $^{40}Ar/^{39}Ar$ phengite ages from unaltered or weakly retrogressed rocks (243–231 Ma, n=3), suggesting that peak PT conditions (530°C at 2.2 GPa; Figure 6a) were attained prior to 240 Ma. Ages for phengites from retrograde, high-strain zones are 224–195 Ma (n=5, including the ~215 Ma age of our station D539; excluding one 187 Ma age). The weak deformation recorded by the pristine mineral assemblage (e.g., porphyroblastic garnet, omphacite, and phengite) and the high-strain fabric traced by the retrograde minerals (e.g., strongly aligned chlorite, amphibole, and epidote) indicate that deformation along the Huwan shear zone occurred mostly during decompression, likely during passage through the crust.

Huwan mélange

Xiongdian eclogite and garnet amphibolite. The metamorphic fabric in most samples is dominated by porphyroblastic garnet and compositional banding that consists either of ≤90% large garnet porphyroblasts, oriented minor white mica, and quartz, or aligned, short prismatic omphacite accompanied by subordinate barroisite, quartz, and zoisite/clinozoisite. Elliptical inclusions and enveloping foliation suggest syn-tectonic growth of garnet (e.g., Passchier and Trouw, 1996). Accessory phases in eclogite are rutile, pyrite, and apatite. Some eclogites show thorough retrogression with the generation of Chl + Bt + Crb in foliation-parallel domains. A shear-band crenulation cleavage in garnet amphibolite 98181 contains retrograde

Hbl + Czo + Pl ± Ilm in microfold hinges that erased all the eclogite-facies minerals other than rounded, corroded garnet and phengite.

Garnet in eclogite D530c shows prograde compositional zoning with cores and rims of $Alm_{62}Grs_{24}Prp_{14}Sps_{<01}$ and $Alm_{53}Grs_{25}Prp_{21}$ $Sps_{<01}$, respectively. Garnet in eclogite 98185 is unzoned $Alm_{49}Grs_{25}Prp_{24}Sps_{02}$. In retrogressed eclogite 98181, almandine decreases from garnet core to mantle and then increases toward the rim; the pyrope content varies inversely to this and grossular is irregular. *Omphacite* yields jadeite contents of <30–50 mol% (calculation after Banno, 1959) without pronounced zoning. Fe^{3+} contents, calculated from charge balance (Ryburn et al., 1976), are highly variable at 0–75% of Fe_{total}. *Phengite* has Si contents of 3.25–3.45 p.f.u. and a paragonite component of 4–12 mol%. Si contents increase from core to rim, pointing to increasing pressure and/or decreasing temperature during growth (Massonne and Schreyer, 1987). Primary, bluish-green *clinoamphibole* is barroisite and magnesiokatophorite, whereas secondary, olive-green amphibole ranges in composition from edenite and pargasite to magnesiohornblende (classification of Leake et al., 1997). C*linozoisite* composition varies from grain to grain with pistacite contents of 4–16 mol%. Secondary *plagioclase* in the pristine eclogite is $An_{00–03}$ albite, whereas retrogressed eclogite 98181 shows An_{10-12} plagioclase coexisting with magnesiohornblende along retrogressed garnet rims.

Thermobarometric calculations for eclogites 98185 and D530c, using garnet rims, high-jadeite omphacite and high-Si phengite and Waters and Martin's (1993) geobarometer, yielded 1.9–2.1 GPa at 500–600°C. At these pressures, garnet–clinopyroxene thermometry (Krogh, 2000; assuming 50% Fe^{3+} of Fe_{total} in omphacite) indicates temperatures of 520–540°C for 98185 and 580–610°C for D530c. Application of Green and Hellman's (1982) garnet–phengite thermometer gave 650°C (98185) and 750°C (D530c) at 2.0 GPa. The empirical amphibole thermobarometer of Ernst and Liu (1998) supports this estimate, yielding 550–600°C at 2.0–2.4 GPa for primary sodic–calcic amphibole prisms in contact with omphacite in D530c.

For garnet amphibolite 98181, which shows relics of the HP metamorphism and secondary mineral assemblages, the identification of the retrograde paragenesis is crucial. As shown above, the microprobe traverse through garnet reveals eclogitic composition in the core, but a distinct change in composition at the rim adjacent to the amphibolite-facies assemblage Hbl + Pl (An_{10-12}) + Ilm. Combined application of Graham and Powell's (1984) garnet–hornblende thermometer and Kohn and Spear's (1990) garnet–hornblende–plagioclase geobarometer yielded 560–605°C at 1.1–1.2 GPa. Similar pressures were obtained with the GRIPS barometer of Bohlen and Liotta (1986). Temperatures reproduced by the amphibole–plagioclase thermometer of Holland and Blundy (1994) and the Ti-in-hornblende thermometer of Colombi (1988) testify to retrogression under epidote-amphibolite facies conditions.

Xiongdian garnet-mica schist. Mica schist 98182 is interlayered with the Xiongdian eclogite and contains Grt + Phn + Qtz + Czo + Pl ± Ttn ± Rt. The schist shows a lepidoblastic fabric and a compositional layering with quartz-rich bands and layers of white mica. Inclusions in the garnet porphyroblasts are quartz, white mica, titanite, and rutile. Similar to the eclogites, *garnet* shows a prograde compositional zoning with core and rim composition of $Alm_{67}Grs_{25}Prp_{07}Sps_{01}$ and $Alm_{63}Grs_{29}Prp_{7.5}Sps_{0.5}$, respectively. *Phengite* is zoned with increasing Si contents from core to rim (Si_{core}: 3.22 p.f.u.; Si_{rim}: 3.34 p.f.u.) and decreasing paragonite component (10 mol% to <5 mol%). *Plagioclase* is nearly pure albite ($An_{00–01}$). C*linozoisite* yielded a pistacite component of ~14 mol%. Prismatic and anhedral titanite has Al_2O_3 contents of up to 2.5 wt.-% and very low Fe_2O_3 contents of >0.3 wt%.

Compositional zoning in 98182 garnet is similar to eclogitic garnet from the same outcrop (D530c, 98185). Phengite shows a rimward increase in celadonite. Assuming that the rim composition of garnet and associated high-Si phengite record peak metamorphism, we obtain 570–600°C (at 2.0 GPa) using the calibration of Green and Hellmann (1982), matching the estimate from the eclogites. Rutile inclusions in garnet and matrix titanite next to clinozoisite the reaction 3 Grs + 5 Rt + 2 Qtz + H_2O ↔ 5 Ttn + 2 Czo. A calculation of this reaction curve with TWEEQ (Berman, 1991; activity models see Appendix) indicates ~1.8 GPa at 600°C. A recalculation of the curve at 600°C assuming a water activity <1 would slightly lower the metamorphic pressures. However, the high modal abundance of phengite in the mica schist as well as the absence of carbonate rather point to a high water activity.

The ~315 Ma age for zircon overgrowths containing Grt + Omp + Phn inclusions establishes a Late Carboniferous age for eclogite-facies metamorphism in the Xiongdian rocks (see above). The age of the retrograde metamorphic history is more difficult to pin down; the syn-kinematic texture of the epidote-amphibole facies minerals in both eclogite and mica schist suggests Paleozoic retrogression (~305 Ma). Triassic zircon growth and the ~235 Ma phengite age out of the top-N shear band fabric in the Xiongdian gneiss point to a Triassic age for the deformation facilitating late-stage retrogression.

Qinling unit

Dingyuan complex amphibolite–greenschist. Sample D525a shows penetrative foliation and compositional variation with mm-sized mafic and felsic lenses and layers. The mafic sections consist of Cam + Chl + Ep + Ab ± Qtz ± Cal ± Ttn; the felsic layers are Qtz + Ab + Phn + Chl ± Zrn ± Ap. Pale-green, aligned *clinoamphibole* is actinolite and magnesiohornblende with the highest Al-, Ti- and Na contents in crystal cores. *Chlorite* has rather uniform composition with Si contents of 5.38–5.60 p.f.u. and X_{Mg} of 0.54–0.56. Similar to clinoamphibole, *epidote* has a distinct chemical variability, with pistacite contents of 20–36 mol% in different grains. Plagioclase is An_{00-02} albite and *carbonate* is almost pure calcite with minor Mg and Fe. *Phengite* yielded Si contents of 3.28–3.43 p.f.u., with the highest values in the cores. The highest paragonite contents (up to 25 mol%) parallel the high Si contents, whereas X_{Mg} is rather uniform (0.51–0.55). Syn-tectonic titanite shows elevated concentrations of Al_2O_3 (up to 6.2 wt%) and Fe_2O_3 contents of up to 3.0 wt%.

Thermobarometry was performed using the Cam–Chl–Ep–Ab–Qtz thermobarometer of Triboulet et al. (1992), which is based on complex exchange equilibria (i.e. tremolite–edenite and pargasite/hastingsite–edenite) between amphibole and associated minerals. Using the midpoint method of Papike et al. (1974) for the calculation of the Fe^{3+} content of amphibole, we obtained peak temperatures of 480°C at 0.7 GPa for amphibole, epidote, and chlorite cores. Calculations based on the maximum and minimum possible Fe^{3+} concentrations in amphibole resulted in errors of ±30°C and ±0.1 GPa. The lowest PT conditions were recorded for hornblende rims and adjacent epidote and chlorite crystals, for which Triboulet et al.'s (1992) thermometer yielded 420°C at 0.4 GPa. Temperatures from the Ti-in-amphibole thermometer of Colombi (1988) are 485°C (core) to 430°C (rim). Metamorphic pressures are given by the elevated celadonite component of phengite in the felsic layers; Si contents >3.4 p.f.u. indicate minimum pressures of about 0.7 GPa at 450°C (Massonne and Szpurka, 1997), whereas lower rim Si contents of <3.35 p.f.u. highlight the retrograde PT path.

The Dingyuan metavolcanic rocks are part of the ~400 Ma magmatic arc (Sm/Nd and Rb/Sr geochronology, see above) and our PT data characterize its regional contact metamorphism. Syn-kinematic white mica in mylonitic rocks related to the Huwan shear zone is ~240 Ma; we suggest that the retrograde overprint concentrated along shear zones is related to deformation associated with the Huwan detachment.

Guishan amphibolites. These are medium-grained rocks, displaying a foliated, mainly nematoblastic microfabric formed by aligned brownish hornblende and subordinate biotite among equigranular plagioclase and quartz. Quartz in compositionally banded amphibolite D527e also forms large, rounded porphyroclasts, suggesting a tuffaceous protolith. Sample D527d features mm-sized, irregular retrogression spots formed by aggregates of pumpellyite, epidote, phengite, and chlorite. Accessories in the amphibolites are ilmenite, titanite, and apatite. *Clinoamphibole* in D527d is pargasite and edenite with elevated TiO_2 contents of up to 1.5 wt%, whereas D527e bears magnesiohastingsite with TiO_2 contents up to 1.1 wt%. Clinoamphiboles of both samples are characterized by elevated K_2O contents of up to 1.8

wt%. Al and Ti contents varies distinctly within the compositional layers and decrease slightly rimward. Individual *plagioclase* are unzoned, but vary from An_{32} to An_{41}. *Biotite* of D527e has high TiO_2 contents (3.5–3.9 wt%) and uniform X_{Mg} values of ~0.46. *Epidote* in the retrograde sections of D527d has pistacite contents of 15–25 mol%, whereas associated *pumpellyite* is a Mg-Al variety (classification of Passaglia and Gottardi, 1973) typical of blueschists (Terabayashi, 1988). *Phengite* yielded Si contents of 3.25–3.45 p.f.u. and shows distinctly variable X_{Mg} values of 0.27–0.82, and secondary c*hlorite* gave Si contents of 5.50–5.61 p.f.u. and X_{Mg} = 0.55–0.58.

Applying the thermobarometer of Ernst and Liu (1998) to amphibole cores of D527d gave 0.85–1.05 GPa at 700–780°C. D527e amphibole core reveal 640–720°C at 1.0–1.2 GPa; similar temperatures are reproduced by the thermometers of Colombi (1988) and Holland and Blundy (1994). These data highlight upper amphibolite- to granulite-facies conditions. Rimward decreasing Ti and Al contents in amphiboles record decreasing PT conditions. The stability of pumpellyite and the pistacite content of coexisting epidote (Maryuama et al., 1986) in the retrogression spots of D527d provide temperature of 250–300°C. The breakdown curve of pumpellyite gives an upper pressure limit of 0.65 GPa (Evans, 1990) and phengite with Si contents of 3.45 p.f.u. constrain a minimum pressures ~0.4 GPa (Massonne and Szpurka, 1997). This PT estimate and the pumpellyite composition indicate low-grade HP/LT conditions typical of subduction zones.

Zircon and white mica geochronology positions the Guishan meta-igneous rocks into the ~400 Ma magmatic arc (see geochronology above). Our K-feldspar age for D527 and neighboring K-feldspar and muscovite ages assign the static blueschist-facies overprint to the Triassic.

Erlangping unit

Erlangping amphibole schist D522a shows a weak foliation obscured by a strongly recrystallized matrix of Cam + Chl + Ep + Ab ± Ilm ± Ap. *Clinoamphibole* is distinctly zoned, with Al, Ti, and Na contents that increase at the expense of Si from actinolite cores to magnesiohornblende rims (Leake et al., 1997). *Chlorite* yielded Si contents of 5.30–5.60 p.f.u. and X_{Mg} values of 0.58–0.62. Whereas small *epidote* crystals show uniform pistacite components of 13–15 mol%, larger crystals yield pistacite contents of ~25 mol% in cores and ~12 mol% in rims. *Plagioclase* forms lens-shaped matrix grains and is An_{00-03} albite. Syn-tectonic and unoriented, recrystallized *phengite* yielded Si contents of 3.15–3.21 p.f.u. with

X_{Mg} values of 0.59–0.67 that vary from grain to grain; BaO reaches 1.3 wt% and paragonite contents are ~ 2 mol%.

The prograde zoning in hornblende allows the calculation of a segment of the metamorphic loop. Applying the thermobarometer of Triboulet et al. (1992) to the actinolitic cores, gives 350–375°C at 0.9-1.0 GPa, which indicates the prograde, clockwise PT evolution of the sample. The same thermobarometer gives maximum PT conditions of 555°C at 0.63 GPa for magnesiohornblende rims and associated epidote and chlorite. Pressures determined from the geobarometer of Cho (cited on page 442 in Laird, 1982) result in a well-defined range of 0.55 to 0.65 GPa for amphibole–chlorite equilibria. Colombi's (1988) thermometer gave 500–560°C for the Ti-rich rims.

Hornblende geochronology in Tongbai suggests that the syn-tectonic metamorphism is ~400 Ma. It likely affected an older (~480 (?) Ma, see geochronology above) igneous protolith.

STRUCTURE AND KINEMATICS

Methods

In the field, we characterized the contacts of the main rock units along traverses by studying the relative amount of deformation, the sense of displacement or shear, and the PT of deformation. The amount of deformation was judged from the shape of deformed objects, the thickness and spacing of deformed zones, and the degree of grain-size reduction. Sense of shear was established in the field and in thin section by means of criteria such as offset markers, σ and δ clasts, shear bands, asymmetric boudinage, schistosité-cisaillement (S-C) fabrics, and lattice-preferred orientation (texture) measurements of quartz. Our quartz-texture interpretation is based on comparisons with textures from deformation zones where the path and temperature have been established by independent criteria, and from polycrystal-plasticity models and experimental data. To understand the kinematics of fault arrays, we applied "stress" inversion techniques to mesoscopic fault-slip data. We refer the reader to Angelier (1994), Passchier and Trouw (1996), and Twiss and Unruh (1998) for comprehensive summaries and critical discussions of these structural methods. Our data are shown in Figures 5 (Cretaceous and Cenozoic deformation) and 7 (Paleozoic and Triassic deformation).

Xinxian complex

Stations D537–538, D539, and D230 record Triassic deformation related to the Huwan shear zone along the very northern margin of the Xinxian complex (Fig. 7a); we did not observe pre-Triassic deformation in this complex. Adjacent stations D537–538, in non-mylonitic felsic gneiss with local mica-rich layers, garnet-mica schist, retrograde, low-grade, quartz-ribbon phyllonite, and small amphibolitized eclogite lenses show spectacular extensional shear bands. The near-vertical, locally overturned, top-NNE fabric indicates post-shear tilting. Syn-kinematic phengite yielded ~235 Ma (this study). Station D539, felsic orthogneiss and garnet-mica schist surrounding amphibolite (relict eclogite), shows top-N shear bands with <a> slip along basal and prism planes in quartz; its late-stage (greenschist-grade) deformation is dated at ~215 Ma (this study). D230, mostly mylonitic, partly chloritic, biotite-orthogneiss, shows top-NE, dextral-normal slip.

Huwan mélange

Stations D530 and D540 of this study, D231 of Hacker et al. (2000) and D335, D339 and D340 of Webb et al. (1999, 2001) record Triassic deformation related to the Huwan shear zone within the Huwan mélange; no older deformation has been quantified (Fig. 7a). Station D530, including one of the Xiongdian eclogite bodies, is in non-mylonitic quartzofeldspathic gneisses with asymmetric foliation boudinage and a dominant synthetic shear-zone set with top-NNW flow. The deformation fabric formed when the footwall was rising and these structures were tilted northward. Early top-NW shear zones dip steeply N and conjugate shear zones dip shallowly S; late shear zones dip more shallowly to the N. Folds with sub-horizontal, W-trending axes and sub-horizontal axial planes overprint all structures. Folding affected steeply N-dipping layering and likely records sub-vertical shortening and sub-horizontal N–S extension during late-stage activity along the then steeply dipping Huwan shear zone (compare Froitzheim, 1992 for similar structures in the Alps). The fabric in both of these stations and adjacent station D335 of Webb et al. (1999) formed late in the metamorphic history, clearly post-dating the Carboniferous HP metamorphism and coinciding with the 263–233 Ma phengite ages and the ~216 Ma zircon rim age obtained from the Xiongdian eclogite area (see above). Station D540, in strongly foliated, locally mylonitic granitic gneiss containing fine-grained amphibolite boudins and dikes (possibly relict eclogite) and intruded by Cretaceous (?) subvolcanic diorite, shows greenschist-facies top-NE flow; the flow direction is poorly constrained. Top-NNE shear in Webb et al.'s (2001) station D340 is well dated between 236 and 230 Ma by Rb/Sr and $^{40}Ar/^{39}Ar$ white-mica ages (see above; Ye et al., 1993; Xu et al., 2000).

Dingyuan complex

The southern margin of the Dingyuan complex is sub-vertical or steeply N-dipping in most localities we visited. Station D525, in relict amphibolite layers in greenschist, and D232 (Webb et al., 1999), in mylonitic quartzofeldspathic schist, have sub-vertical shear zones and shear bands with top-N(E) flow, again suggesting that the deformation fabric was tilted northward during footwall uplift. Phengite in the low-T, top-N mylonite of D232 dates deformation at ~235 Ma (Webb et al., 1999).

Nanwan and Foziling unit

Huwan detachment deformation dies out within the southern part of the Nanwan unit. All stations we analyzed show sub-vertical fabrics and record Triassic deformation related to the Huwan shear zone; no older deformation has been quantified. Ductile-to-brittle faults in station D526 are interpreted to have formed when the foliation and bedding was subhorizontal or shallowly N-dipping; displacement was then top-N. Station D535 just north of the Dingyuan–Nanwan boundary shows steeply N-dipping, top-S shear bands and shears zones resulting in foliation boudinage; in the Chinese literature deformation of these well-bedded, phyllitic quartzites and chloritic quartzose phyllites is interpreted as top-S thrusting of the Nanwan unit onto the Dingyuan complex (e.g., Xu et al., 2000). In contrast, we suggest that an initially shallowly S-dipping, top-S extensional shear fabric, antithetic to the top-N shear along the Huwan detachment (and likely along the Dingyuan–Nanwan contact, not exposed at D535) was rotated into the apparent thrust geometry by large-scale N–S extension and later folding. Deformation during cooling, the excision of Triassic isograds across the Huwan detachment, and the progressive rotation of the deformation fabrics, as observed at several outcrops (e.g., D530), support the sub-horizontal extension interpretation (see discussion below). The greenschist-facies pelites (phyllite and quartzose phyllite) of station D532, just north of the boundary to the Dingyuan complex, are tightly folded and overprinted by ductile–brittle fault zones with top-N shear; this station likely portrays deformation along the northern margin of the Huwan shear zone. Station D528 records tight upright folding within the

Nanwan complex; the relationship of this folding to normal shear along the Huwan detachment is unclear.

In the northern Dabie foreland, six stations portray Permo–Triassic, low-T deformation (Fig. 7b; muscovite cooling ages of 271 and 261 Ma, Figure 2a) in the Foziling unit. Quartzite (D542, D543), partly mylonitic quartzose phyllite (D544) with <a> folds, and volcaniclastic, quartzose two-mica gneiss (D544), show variable but mostly vertical foliation, indicating folding with SE-trending axes. Unfolding suggest coaxial sub-horizontal extension along the NW–SE mineral lineation with a non-coaxial top-NW component. Stations D546 and D547, (chlorite–)biotite quartz schists, are close to the Luzhenguan–Foziling contact and show dextral strike-slip (D546) and top-NNW (D547) shear; unfolding suggest top-NW normal faulting for both stations, corroborating the interpretation of Hacker et al. (2000) of that contact; their ~242 Ma phengite is syn-kinematic.

Guishan complex

Station D222 in the Guishan complex (Fig. 7a) consists of partly mylonitic amphibolite with leucocratic layers and metavolcaniclastic rocks. It has a vertical foliation and shear-band fabric with sinistral shear under amphibolite- to retrograde greenschist-facies conditions, all overprinted by active sinistral strike-slip faults. Early isoclinal <a> folds indicate high strain, and second-generation folds are strongly asymmetric and related to the sinistral shear. As these rocks were overprinted by Cretaceous regional metamorphism (K-feldspar age of ~100 Ma), the recorded deformation is older, likely Paleozoic.

Stations D517–518, D519, and D527 characterize the deformation in the Guishan complex of northeastern Tongbai near Xinyang (Fig. 7a). Nearby stations D517–D518 consist of locally kyanite–staurolite bearing micaschist and gneiss, marble, mylonite with feldspar and hornblende blasts, and its retrograde products; this sequence is interpreted as intercalated volcaniclastic rocks and limestone. Deformation began at amphibolite-facies conditions and continued during cooling through ductile–brittle shearing/faulting; isoclinal folds and late open folds are present. An early conjugate set of shear bands indicates strong coaxial NE–SW shortening within the then-vertical foliation; the shear bands were later rotated into their apparent normal fault geometry. A second set of shear zones were then imprinted, again indicating NE–SW contraction. Given the 316 to 401 Ma $^{40}Ar/^{39}Ar$ hornblende ages in the Guishan complex of northwestern Tongbai, the ductile deformation is likely Paleozoic; the outcrop at station D518 is cut by a probable Cretaceous dike that shows only brittle deformation. Station D519 is an L-tectonite orthogneiss with a similar structural pattern to D517–518; this gneiss likely yielded the 392 Ma protolith age reported by Ye et al. (1993). Station D527 just north of the boundary to the Nanwan unit contains retrograde hornblende, tourmaline, and K-feldspar bearing biotite gneiss and garnet-bearing amphibolite. An early mylonitic deformation developed during sinistral strike-slip flow was overprinted by HP/LT metamorphism (see above). Niu et al.'s (1994) hornblende age of ~401 Ma dates deformation as Early Devonian and our K-feldspar age of ~240 Ma indicates that the HP/LT overprint was Triassic.

Erlangping unit

Stations D520–D521 lie in a spectacular sinistral strike-slip shear zone along the boundary between the Guishan complex and the Erlangping unit, in gabbro (partly retrogressed to talc-schist), serpentinized ultramafic rock, and mylonitic orthogneiss (Fig. 7a). Greenschist-grade mylonitization resulted in mostly symmetric boudinage of greenschist in a carbonate matrix and progressed into ductile–brittle faulting, expressed as flexural folds accommodating faults with calcite fibers. This zone is overprinted by later brittle, possibly active faulting (see below). ~400 Ma hornblende ages farther west constrain the ductile deformation as Early Devonian. Station D533 shows a partly mylonitized, strongly boudinaged sequence of thick, well-bedded marble and amphibolite–greenschist (Fig. 7a). High strain in a sinistral strike-slip setting is also indicated by isoclinal <a> type flow folds; the structures are refolded by open folds.

Cretaceous and Cenozoic structures

Stations D523 and D525–526 record Early Cretaceous (nearby 128–120 Ma biotite cooling ages) sub-horizontal extension (Fig. 5a). At station D523 felsic orthogneiss, K-feldspar rich granite, and pegmatite dikes intrude amphibolite–micaschist intercalations (likely relics of Huwan mélange rocks); the intrusions resemble the Northern Orthogneiss unit of Dabie. Station D522 exemplifies the stress field in place during Late Cretaceous–Early Tertiary deformation, which is concentrated along the dextral Tongbai shear-fault zone (Webb et al., 1999; Ratschbacher et al., 2000). This shear–fault zone is associated with Upper Cretaceous, possibly lower Tertiary (K_2 on Chinese maps) basins. In Tongbai, $^{40}Ar/^{39}Ar$

biotite cooling and pseudotachylite ages (Webb et al., 1999) suggest (re)activation of the Tongbai shear zone at ~75 Ma.

Cenozoic faulting is concentrated along the Jinzhai fault in northernmost Xinxian and Tongbai and along the Tongbai shear–fault zone. Both fault zones are sinistral, and the Jinzhai fault is definitely active, as indicated by Recent geomorphic features (e.g., Zhang et al., 1995). Evidence of the associated regional stress field (NW–SE extension, NE–SW compression) was encountered at nearly every location visited, but accommodated strain is low. Dextral faults, conjugate to the sinistral strike-slip faults, strike NNE and are transtensional. Such faults are active in the Dabie Shan (Zhang et al., 1995; Ratschbacher et al., 2000) and define the NNE-trending boundaries of blocks that segment the Hong'an–Dabie area into basement massifs and basins. A Tertiary faulting history is indicated by the early Tertiary AFT ages along the Tongbai fault.

DISCUSSION

Location of the Sino-Korean–Yangtze suture and role of Carboniferous high-pressure metamorphism in the Qinling–Dabie orogen

The Tongbai–Xinxian–northern Dabie area contains three sutures (Fig. 2a): (1) The SKC–Erlangping intra-oceanic arc suture is younger than the intra-oceanic arc rocks (~480 Ma, but poorly defined in Tongbai–Xinxian) and older than the Silurian–Devonian arc rocks stitching the SKC (Kuanping unit), the Erlangping and Qinling units. (2) The Erlangping arc–Qinling unit suture has the same time constraints. (3) The Qinling unit–YC suture formed at ≥240 Ma, based upon the oldest ages of HP–UHP metamorphism in the northern YC.

We resolve the controversies about the age of the SKC–YC collision by suggesting that the Paleozoic collisions occurred between the Qinling unit and the SKC, post-dating the amalgamation of the intervening Erlangping arc with these continental units. The Qinling unit constitutes a long and narrow microcontinent that extends at least through Qinling–Dabie; Hacker et al. (2005) suggested that the Qinling microcontinent continues into the Sulu area. A suite of common characteristics delineate this microcontinent throughout the Qinling, Tongbai–Xinxian, and northern Dabie areas: (1) These areas experienced the Mesoproterozoic (~1.0 Ga) Jinningian orogeny that assembled Rodinia (Fig. 3a,b; Li, 1999; Li et al., 2002). (2) They share the ~0.8–0.7 Ga rifting event that marks Rodinia's breakup (Fig. 3a,b; e.g., Li Z.X. et al., 1995, 1999). In Xinxian and northern Dabie, portions of the Dingyuan and

Luzhenguan complexes hold the magmatic signature of this rifting event: quartzofeldspathic rocks (former volcanic and volcaniclastic rocks) intercalated with amphibolite (former mafic volcanic rocks), and granitoids, the intrusive part of the volcanic series. (3) Most importantly, these areas share the arc that developed on the Proterozoic microcontinent and northern collage (Erlangping unit and SKC) in the Late Silurian–Early Devonian (Fig. 3a,b). In the Qinling, the arc sequence is mostly plutonic, as it is in Tongbai, where it is represented by, for example, the large Huanggang quartz diorite complex. Most of the Guishan and Dingyuan rocks in Xinxian seem to have been emplaced as volcanic rocks and were metamorphosed to up to granulite facies during regional metamorphism accompanying arc development, a local metamorphic signature the Xinxian rocks share with those in Tongbai. No direct record of Silurian–Devonian arc rocks is known from the Luzhenguan unit, which seems to represent only the Neoproterozoic rift.

The Proterozoic history of the Qinling microcontinent also ties it to the YC, and this has hindered the recognition of the Qinling unit as a separate microcontinent that lies between the SKC and the YC all along the Qinling–Dabie–Sulu orogen. The Jinningian orogeny and the Neoproterozoic rifting were defined in the YC. The north(west)ern margin of the YC also suggests that the Neoproterozoic "rifting event" actually marks two distinct events that are difficult to separate based only on age, and particularly so in the Qinling microcontinent, where the geochronological data base is limited and obscured by the overprinting Paleozoic arc. Local, petrochemically well-studied granitoids define an older age group at ~815 Ma that constitutes the Panxi–Hannan arc (e.g., Zhou et al., 2002), whereas a larger and better-defined group at ~732 Ma corresponds to rifting of Rodinia (e.g., Gao et al., 1990).

So it is the Paleozoic signature that undoubtedly differentiates the Qinling microcontinent from the YC; this signature includes the Silurian–Devonian arc but also older components, e.g., the ~580 Ma Sujiahe gabbro and other, possibly coeval, gabbros that dot the Dingyuan complex and which may hint to an Early Paleozoic subduction history. It is also the presence of a Paleozoic fore-arc basin on the Qinling microcontinent and the occurrence of the Huwan mélange (see below).

The Qinling microcontinent and its arc carry an incompletely preserved fore-arc basin, constituted by the Liuling unit of Qinling (or part of it), the Nanwan unit of Xinxian, and the Foziling unit of Dabie. We suggest a fore-arc setting due to the position of these units on the southern margin of the main volume of the presently exposed arc rocks and the presence of continental basement beneath them, indicated most clearly by the Guishan and Dingyuan complexes in Xinxian and the Luzhenguan complex in Dabie. Furthermore, detrital geochronology ties the Liuling and Foziling units to the Qinling microcontinent and its Paleozoic arc: both units carry the ~400 and 700–800 Ma arc and rift signature of the Qinling microcontinent; the Liuling unit also shows the 1.0 Ga orogenic event. The ~400 Ma detrital zircon ages in the Foziling unit are important, as they indicate the presence of the Silurian–Devonian arc in the hinterland, for which evidence is lacking in the Qinling "basement", the underlying Luzhenguan complex (see above).

The geochronology of arc magmatism seems to imply that northward subduction beneath the Qinling microcontinent terminated during the Devonian. However, fossiliferous units in the Liuling unit reach up into the Lower Carboniferous. Furthermore, the paucity of volcanic rocks in most of the Nanwan and Foziling units and also the apparent lack of volcanic rocks in the Carboniferous rocks that apparently overlie them suggest that the fore-arc basin partly postdates arc activity. The apparent end of arc magmatism on the Qinling microcontinent and the Erlangping unit remains to be explained and may simply reflect a change in subduction geometry in the Paleotethys ocean.

The Huwan mélange and the geochronology of the hanging wall serve as the bridge to tie the Paleozoic evolution of the collage along the southern margin of the SKC (Erlangping and Qinling units) to the subduction of the leading edge of the YC. We interpret the Huwan mélange as a Carboniferous–Permian (and likely older) subduction–accretion complex with a tectonic and possibly sedimentary mixture of rocks from the Qinling microcontinent, the Silurian–Devonian arc, the Paleotethyan ocean floor, and the YC. Most importantly, the eclogites involved in the mélange signify oceanic subduction during the Carboniferous (their age of HP metamorphism). The geochemistry of some of the Huwan eclogites (e.g., Xiongdian) indicates that they are oceanic basalts, implying that they cannot be blocks scraped off the YC, as such rocks do not exist in the YC (see the studies on the origin of the Hong'an–Dabie eclogites, e.g., Jahn, 1998 and discussion on the Dabie Shan below). Other eclogites, such as the Hujiawan eclogite, seem to have magmatic arc affinity: The geochemistry, position along the northern margin of the Huwan mélange, and the Neoproterozoic and Paleozoic age components of the Hujiawan eclogite hint that this group of eclogites may constitute tuffs derived from the Silurian–Devonian arc. Other eclogites, such as the Qianjinhepeng eclogite with its 0.93 Ga and in particular the strong 0.72 Ga age component, may derive from the YC. Again, the Qianjinhepeng eclogite position along the northern edge of the Huwan mélange and its Paleozoic age component make a Qinling origin more likely.

The age of HP metamorphism in the Huwan-mélange eclogites ranges from 325–312 Ma and does not span the proposed Paleozoic–Early Triassic subduction–accretion history. This may be the result of incomplete preservation or insufficient investigation. For example, Devonian to Permian zircon spot ages reported from the Xiongdian quartz-eclogite (see geochronology above) may reflect subduction-related recrystallization/metasomatism throughout the Late Paleozoic in the Huwan mélange. This is supported by the range of cooling ages in the Nanwan and Foziling units (271–204 Ma)—which we interpret as the fore-arc—and in the Erlangping and Qinling units of Tongbai–Xinxian (316–234 Ma) that signify Early Permian–Triassic and early Late Carboniferous–Triassic thermal events.

Whether arc magmatism ended in the Silurian–Devonian remains to be tested: It is possible that Middle Carboniferous–Early Permian andesitic breccia and tuff in the eastern half of the SKC (e.g., Zhang, 1997) may signify northward migration of the arc in the central part of the orogen, and that at least some of the Permo–Triassic plutons within the eastern Songpan–Garzê flysch belt are subduction related (Ratschbacher et al., 2003).

Why does the Silurian–Devonian arc signature diminish from Qinling–Tongbai–Xinxian into Dabie and why is the arc apparently not present in Sulu? The paleomagnetic record shows that convergence and collision between the SKC and YC involved a clockwise rotation of up to 70° (e.g. Zhao and Coe, 1987; Gilder et al., 1999). Thus, one might speculate that the Paleotethys ocean south of the SKC narrowed eastward (into the Dabie–Sulu area) and that no arc formed in the east (compare Li et al., 2001).

Finally, and speculatively, the eclogites associated with mantle-derived ultramafic rocks in the northern Northern Orthogneiss unit (type III eclogites of Jahn, 1998) of Dabie may be in an analogous structural position to the Huwan mélange rocks. Thus, it may be that the Qinling microcontinent–YC suture, here drawn along the Cretaceous Xiaotian–Mozitang shear–fault zone, south of the Foziling and Luzhenguan units in northern Dabie should be drawn farther south within the Northern Orthogneiss unit (the thin dotted line in Fig. 2a).

Pressure–temperature–time–deformation history of the Huwan detachment

Structural studies have not yet precisely located the boundaries of the Huwan shear–fault zone definitively. Our observations along a few transects suggest that high strain associated with the detachment sets in and overprints strong, often penetrative deformation in the YC rocks along the very northern margin of the northern Dabie–Xinxian complex. We did not find high-strain ductile or brittle deformation related to Huwan normal shear north of the southern margin of the Nanwan unit in Xinxian; the Foziling unit is affected heterogeneously by normal shear. Thus, we tentatively place the northern margin of the Huwan detachment along the southern margin of the Nanwan unit.

We emphasize that the Huwan detachment is not the only high-strain shear zone involved in exhuming the HP–UHP rocks: the entire basement core of the Hong'an–Dabie orogen is strongly deformed (see Hacker et al., 2000; Webb et al., 1999, 2001 for structural data) and low-strain regions are confined to mm- to multiple-km-scale boudins, hosting most of the HP–UHP evidence (for a spectacular example in Dabie see Oberhänsli et al., 2002). Our observations also suggest that in general strain is weaker in those parts of the Huwan detachment that preserve the HP assemblages (both in the Huwan mélange and the Northern Dabie–Xinxian complex) than in retrograde shear zones that are often mylonitic. Although the outcrops we found did not allow us to describe deformation represented by syn-HP structures quantitatively (e.g., in terms of vorticity, strain, rheology), these structures show similar overall orientation than the retrograde ones. The HP structures they seem, however, to widely lack the non-coaxial flow criteria that are ubiquitous in the retrograde, high-strain portion of the detachment. Furthermore, our overall impression from relating critical mineral assemblages to deformation is that the Huwan high-strain deformation describes passage of rocks through crustal section of the lithosphere.

The Huwan detachment deformation is sub-horizontal N–S extension and vertical shortening. That this deformation produced crustal thinning is clear from i) the overall structural geometry (N-dipping flow planes and top-N kinematics), ii) the shortening of isograds across the detachment (Triassic pressures of ~0.4 GPa in the Dingyuan greenschist contrast with ~2.2 GPa along the northern margin of the Xinxian complex), and iii) the fact that deformation post-dated the peak pressures. Although the nature of the initial contacts of the major units (the Xinxian complex, Huwan mélange, Dingyuan complex, and Nanwan unit) that the Huwan shear zone overprints are structurally undefined, the Triassic deformation is normal shear; local apparent thrust geometries within the Huwan shear zone are the result of rotation due to footwall uplift. Our petrologic work confirmed the suggestion that the coesite-bearing UHP core of Hong'an is rimmed in the north by a HP zone. Assuming a pressure difference of Triassic metamorphism of ~1.6 GPa (~2.0 GPa or ~70 km depth in the Xinxian complex and ~0.4 GPa or ~15 km in the Dingyuan complex) at the onset of deformation along the Huwan detachment and a ~45° dip to the shear zone results in ~80 km displacement along the fault and ~55 km subhorizontal extension.

The Huwan detachment deformation was Triassic. As argued above, we suggest that the peak pressure predated 240 Ma. In the Xinxian complex, syn-kinematic phengite grew in mylonitic shear zones as early as ~235 Ma; late-stage high-strain shear was active at ~215 Ma. In the Huwan mélange and the Dingyuan complex, early top-N(NE) shear that can be clearly attributed to the Huwan detachment is 236–230 Ma; shear along the Luzhenguan–Foziling contact began as early as 242 Ma. We thus propose that deformation along the Huwan shear zone initiated at ~235 Ma. The main body of retrograde phengite ages within the Huwan shear zone is 224–195 Ma, bracketing its major activity. Rates of exhumation of ~1.9 and ~1.4 mm/a apply taking 31 Ma (224–195 Ma) and 40 Ma (235–195 Ma), respectively, for passage of rocks through ~55 km (see above); these are rates observed in active orogens today.

Pressure–temperature–time–deformation history of the Xinxian–Dabie foreland (north of the Huwan detachment)

Our petrology and the available geochronology outline middle–lower crustal "regional contact metamorphism" in rocks of the Silurian–Devonian arc at ~400 Ma (Ratschbacher et al., 2003). Our peak PT estimates (680–740°C at 0.9–1.1 GPa) for the Guishan complex are similar to those derived from Qinling microcontinent rocks in Qinling (0.9–1.0 GPa at 700–800°C; e.g., Hu et al., 1993) and the garnet granulites in northwestern Tongbai (~0.97 GPa and 755–840°C; Kröner et al., 1993). Metamorphic grade decreases from granulite facies in the Guishan complex to upper greenschist facies in the Erlangping unit. In Xinxian, a wide belt of high-strain sinistral wrench deformation that straddles the Guishan–Erlangping contact developed during but mostly after this ~400 Ma metamorphism. Similar high-strain, sinistral-transpressive mylonite zones have been observed in Qinling (see Ratschbacher et al., 2003); the most spectacular being the sinistral–transpressive Shang–Dan shear–fault zone that was active in the early Devonian (~400 Ma).

The evidence of a static, ~255–240 Ma blueschist metamorphism in the Guishan complex of Tongbai, the 271–204 Ma range of cooling ages in the Nanwan and Foziling fore-arc units, and the 316–234 Ma cooling ages in the Erlangping and Qinling unit of Tongbai–Xinxian are best interpreted as originating from Paleotethys subduction along the Huwan-mélange suture zone (see above). This metamorphic signature is not related to the exhumation along the Huwan detachment, as it extends far north of the Triassic shear zone and is older.

Collision zone overprint in the Cretaceous–Tertiary

Despite its dominance in the Dabie Shan (Ratschbacher et al., 2000, 2003) surprisingly little Early Cretaceous deformation occurred in the Tongbai–Xinxian–Hong'an and Qinling areas. The massive 130–115 Ma cluster of cooling ages in Xinxian–Hong'an thus may simply reflect regional, locally rapid cooling after granitoid injection and regional Cretaceous heating. The intense concentration of Early Cretaceous magmatism along the Triassic Qinling microcontinent–YC suture (the Huwan mélange) in Tongbai–Xinxian and particularly in northern Dabie (Northern Orthogneiss unit) have been interpreted as the result of Pacific subduction (Ratschbacher et al., 2000) or mantle delamination (Wu et al., 2005). In either case it is a spectacular demonstration of the effect that pre-existing heterogeneities can have on a subsequent, unrelated tectonic event.

Late Cretaceous–Early Tertiary deformation along dextral transpressional shear–fault zones and associated basins are a characteristic feature of the entire Qinling–Xinxian–Dabie orogen. Deformation along similar zones has been loosely constrained between 101 and 63 Ma in Qinling (Ratschbacher et al., 2003), at ~75 Ma along the Tongbai shear–fault zone (Webb et al., 2001), and younger than ~115 Ma in Dabie (reactivation of the Xiaotian–Mozitang fault zone in a dextral-transtensional setting; Ratschbacher et al., 2000). The bulk of the AFT ages (80–55 Ma age cluster) are also Late Cretaceous–Early Tertiary and may signify cooling related to transtension during this event; the cooling follows the time of reheating and subsequent cooling documented in Dabie at ~100–90 Ma (Ratschbacher et al, 2000), likely also recorded by the K-feldspar ages of Xinxian (Fig. 3e). Transtension within the Qinling–Dabie orogen coincides with rifting marked by Late Cretaceous–Eocene red bed deposition throughout eastern China (e.g., Ren et al., 2002).

Two major conclusions may be gleaned from the fission-track data: (1) Exhumation rates were slow throughout the Cretaceous–Tertiary; the spectacular exception is the Early Cretaceous exhumation of the Northern Orthogneiss unit of northern Dabie. Our slow average rate of ~0.06 mm/a for the last 70 Ma for Xinxian and the foreland of Dabie is consistent with slow rates of Tertiary exhumation of ~0.02 mm/a for the flanks of the Dabie Shan, and 0.05–0.07 mm/a for the core of the range, derived from (U-Th)/He and AFT ages and considering erosion and topography (Reiners et al., 2003). The Cretaceous period prior to ~70 Ma was likely a time of extremely slow, continuous exhumation and peneplanation for most of the orogen (compare Enkelmann et al., in press). (2) The India–Asia collision may have induced reactivation of pre-existing fault zones in the Eocene; we documented enhanced cooling along the Tanlu fault zone (Grimmer et al., 2002) and along the faults zones in Tongbai–Xinxian (this study). Reiners et al. (2003) suggested a modest increase in exhumation rate within the Dabie Shan between 80 and 40 Ma (≤0.2 mm/a).

CONCLUSIONS

The Qinling–Dabie–Sulu orogen contains three sutures in Tongbai–Xinxian (northern Hong'an)–northern Dabie: The Silurian Sino-Korean Craton–Erlangping intra-oceanic arc suture; the Silurian Erlangping arc–Qinling microcontinent suture; and the Early Triassic Qinling microcontinent –Yangtze Craton suture. This recognition of three sutures resolves the controversies about the age of the Sino-Korean Craton–Yangtze Craton collision by placing the Paleozoic collisions between the Qinling microcontinent and the Sino-Korean Craton, and the Mesozoic collision between the Qinling microcontinent and the Yangtze Craton. The Qinling unit constitutes a long and narrow microcontinent that extends through Qinling–Dabie and probably into Sulu. Its common characteristics in Qinling, Tongbai–Xinxian, and northern Dabie are: ~1.0 Ga orogeny, ~0.8–0.7 Ga arc formation and rifting events, and Late Silurian–Early Devonian (~400 Ma) arc formation. In Xinxian, the arc is represented mostly by volcanic rocks (Guishan and Dingyuan complexes) that were metamorphosed to up to granulite facies (peak: 680–740°C at 0.9–1.1 GPa) during "regional contact metamorphism", this metamorphic signature is also found in Tongbai.

Whereas the Proterozoic history of the Qinling microcontinent ties it to the Yangtze Craton, its Paleozoic arc signature, the presence of a mid-?late Paleozoic (the Liuling–Nanwan–Foziling) fore-arc basin, and the partly oceanic Huwan mélange make the Qinling microcontinent distinct from the Yangtze Craton. Detrital geochronology ties the Liuling and Foziling units to the Qinling microcontinent basement and its Paleozoic arc.

The Huwan mélange is a Carboniferous–Permian (and likely older) subduction–accretion complex containing elements of the northern microcontinent and its arc, the Paleotethyan ocean floor, and possibly the Yangtze Craton. Quartz eclogites (e.g., the 540–590°C and 2.1 GPa Xiongdian eclogite) signify Carboniferous (~315 Ma) subduction. Devonian to Permian zircon spot ages from the eclogites may reflect subduction throughout the Late Paleozoic. This is supported by the 271–204 and 316–234 Ma ranges of $^{40}Ar/^{39}Ar$ and Rb/Sr mineral ages in the fore-arc and its basement, and the static, ~255–240 Ma blueschist metamorphism in the basement of the upper plate.

The high- and ultrahigh-pressure rocks of the Xinxian–Hong'an block (pressure peak at ≥240 Ma) are bounded along their northern margin by the Huwan extensional detachment; the boundaries of this high-strain zone extend from the northernmost Yangtze Craton to the southern margin of the Nanwan unit. The Huwan high-strain deformation describes the passage of rocks through crustal section of the lithosphere by sub-horizontal N–S extension and vertical shortening. This is evident from the condensed Triassic isograds (420°C and ~0.4 GPa in the hanging wall Dingyuan greenschist and ~530°C and 2.2 GPa in the Xinxian complex footwall). Apparent thrust geometries within the Huwan shear zone resulted from rotation due to footwall uplift. The Huwan detachment deformation was Triassic: syn-kinematic phengite grew as early as ~235 Ma, and the main deformation occurred during cooling from 224–195 Ma. Rates of exhumation were 1.9–1.4 mm/a. The Huwan detachment is not the only high-strain shear zone involved in exhumation of the HP–UHP rocks: the entire basement core of Hong'an–Dabie orogen is strongly deformed.

The Tongbai–Xinxian area shows a massive 130–115 Ma cluster of cooling ages, reflecting regional cooling after granitoid injection and regional Cretaceous heating. Apatite fission-track ages cluster at 80–55 Ma and signify cooling related to transtension that coincides with rifting marked by Late Cretaceous–Eocene red bed deposition throughout eastern China. Slow average rates of ~0.06 mm/a for the last 70 Ma characterize Xinxian and Dabie. The Cretaceous period prior to ~70 Ma was likely a time of extremely slow, continuous exhumation and peneplanation for most of the Qinling–Dabie orogen; the spectacular exception is the Northern Orthogneiss unit of northern Dabie. The India–Asia collision reactivated the orogen in the Eocene, particularly along the Tanlu fault zone and locally along the faults zones in Tongbai–Xinxian.

APPENDIX

Activity models used to calculate reaction curves: Omphacite, Holland (1980, 1990); garnet, Hodges and Spear (1982); phengite, titanite, and clinozoisite: ideal (recommendations of Waters and Martin, 1996 and Carswell et al., 2000); quartz, H_2O = 1.

ACKNOWLEDGMENTS

Funded by DFG grants Ra442/19 and 20. Andy Calvert contributed multi-diffusion-domain modeling of K-feldspar sample D222d. The EBSD calcite texture of sample D533 was

measured by Yanxia Xie in the lab of Rudy Wenk. We thank Juhn Liou, Mike McWilliams, and Michael Terry for constructive reviews.

REFERENCES CITED

Ames, L., Zhou, G., and Xiong, B., 1996, Geochronology and geochemistry of ultrahigh-pressure metamorphism with implications for collision of the Sino-Korean and Yangtze cratons, central China: Tectonics, v. 15, p. 472–489.

Angelier, J., 1994, Fault-slip analysis and paleostress reconstruction, *in* Hancock, P.L. ed., Continental Deformation: Pergamon, Tarrytown, N.Y., p. 53–100.

Banno, S., 1959, Aegirine augites from crystalline schists in Sikoku: Journal of the Geological Society of Japan, v. 65, p. 652–657.

Berman, R., 1991, Thermobarometry using multi-equilibrium calculation: a new technique with petrologic applications: Canadian Mineralogist, v. 29, p. 833–855.

Bohlen, S., and Boetcher, A., 1982, The quartz-coesite transformation: a pressure determination and the effects of other components: Journal of Geophysical Research, v. 87, p. 7073–7078.

Bohlen, S., and Liotta, J., 1986, A barometer for garnet amphibolites and garnet granulites: Journal of Petrology, v. 27, p. 1025–1034.

Carswell, D., 1990, Eclogites and the eclogite facies, *in* Carswell, D., ed., Eclogite facies rocks: Blackie, Glasgow, p. 1-13

Carswell, D., O'Brian, P., Wilson, N., and Zhai, M., 1997, Thermobarometry of phengite-bearing eclogites in the Dabie Mountains of central China: Journal of Metamorphic Geology, v. 15, p. 239–252.

Carswell, D., O'Brian, P., Wilson, R., and Zhai, M., 2000, Metamorphic evolution, mineral chemistry and thermobarometry of schists and orthogneisses hosting ultrahigh pressure eclogites in the Dabieshan of central China: Lithos, v. 52, p. 121–155.

Cawthorn, R., and Collerson, K., 1974, The recalculation of pyroxene end-member parameters and the estimation of ferrous and ferric iron content from electron microprobe analyses: American Mineralogist, v. 59, p. 1203–1208.

Chen, J., Dong, S., Deng, Y., and Chen, Y., 1993, Interpretation of K-Ar ages of the Dabie orogen–a differential uplifted block: Geological Review, v. 39, p. 15–22.

Chen, J.-F., Xie, Z., Liu, S.-S., 1995, cooling ages of the Dabie orogen, China, determined by ^{40}Ar-^{39}Ar and fission track techniques: Science in China (Series B), v. 38, p. 749–757.

Chen, D., Wu, Y., Wang, Y.-J., Zhi, X., Xia, Q., and Yang, J., 1998, Ages, Nd and Sr isotopic compositions of the Jiaoziyan gabbroic intrusion from the northern Dabie terrain: Scientia Geologica Sinica, v. 7, p. 29–35.

Chen, F., Guo, J.-H., Jiang, L.-L., Siebel, W., Cong, B., and Satir, M., 2003, Provenance of the Beihuaiyang lower-grade metamorphic zone of the Dabie ultrahigh-pressure collision orogen, China: evidence from zircon ages: Journal of Asian Earth Sciences, v. 22, p. 343-352.

Colombi, A., 1988, Métamorphisme et géohemie des roches mafiques des Alpes ouest-centrales (géopofil Viège Domodossola-Locarno): Ph.D. thesis, University Lausanne (CH), 216 p.

Cui, W., and Wang, X., 1995, Eclogites of southern Henan and northern Hubei province, central China: The Island Arc, v. 4, p. 347–361.

Droop, G.T.B., 1987, A general equation for estimating Fe^{3+} concentrations in ferromagnesian silicates and oxides from microprobe analyses, using stoichiometric criteria: Mineralogical Magazine, v. 51, p. 431–435.

Eide, E. and Liou, J. G., 2000, High-pressure blueschists and eclogites in Hong'an: A framework: Lithos, v. 52, p. 1–22.

Eide, E., McWilliams, M. O., and Liou, J. G., 1994, $^{40}Ar/^{39}Ar$ geochronologic constraints on the exhumation of HP-UHP metamorphic rocks in east-central China: Geology, v. 22, p. 601–604.

Enkelmann, E., Jonckheere, R., and Ratschbacher, L., 2005, The effects of radiation damage accumulation and annealing on fission-track dating of titanite: Nuclear Instruments and Methods in Physics Research, Section B, v. 227, p. 567–576.

Enkelmann, E., Ratschbacher, L., Jonckheere, R., Gloaguen, R., Nestler, R., Fleischer, M., Hacker, B. R., Zhang, Y., in press, Is Tibetan lower crustal flow diverging around the Sichuan basin? Denudation and deformation in the Qinling: Geological Society of America, Bulletin.

Ernst, W., and Liou, J. G., 1998, Experimental phase-equilibrium study of Al and Ti contents of calcic amphibole in MORB - a semiquantitative thermobarometer: American Mineralogist, v. 83, p. 952–969.

Evans, B., 1990, Phase relations of epidote blueschists, *in* Okrusch M., ed., Third International Eclogite Conference, Lithos, v. 25, p. 3-23.

Faure, M., Sun, Y., Shu, L., Monié, P., and Charvet, J., 1996, Extensional tectonics within a subduction-type orogen : The case study of the Wugongshan dome (Jiangxi Province, SE China): Tectonophysics, v. 263, p. 77–108, 1996.

Faure, M., Lin, W., Shu, L., Sun, Y., and Schärer, U., 1999, Tectonics of the Dabieshan (eastern China) and possible exhumation mechanism of ultra high-pressure rocks: Terra Nova, v. 11, p. 251–258.

Faure, M., Lin, W., and Le Breton, N., 2001, Where is the North China–South China block boundary in eastern China?: Geology, v. 29, p. 119–122.

Faure, M., Lin, W., Monié, P., Le Breton, N., Poussineau, S., Panis, D., and Deloule, E. 2003, Exhumation tectonics of the ultrahigh-pressure metamorphic rocks in the Qinling orogen in east China: New petrological-structural-radiometric insights from the Shandong Peninsula: Tectonics, v . 22, doi10.1029/2002TC001450.

Franz, L., Romer, R., Klemd, R., Schmid, R., Oberhänsli, R., Wagner, T., and Dong, S., 2001, Eclogite-facies quartz veins within metabasites of the Dabie Shan (eastern China): pressure-temperature-time-deformation-path, composition of the fluid phase and fluid flow during exhumation of high-pressure rocks: Contributions to Mineralogy and Petrology, v. 141, p. 322–346.

Frimmel, H.E., and Frank, W., 1998, Neoproterozoic tectono–thermal evolution of the Gariep Belt and its basement, Namibia and South Africa: Precambrian Research, v. 90, p. 1–28.

Froitzheim, N., 1992, Formation of recumbent folds during synorogenic crustal extension (Austroalpine nappes, Switzerland): Geology, v. 20, p. 923–926.

Fu, B., Zheng, Y.-F., and Touret, J.L.R., 2002, Petrological, isotopic and fluid inclusion studies of eclogites from Sujiahe, NW Dabie Shan (China): Chemical Geology, v. 187, p. 107–128.

Gao, S., Zheng, B., Li, Z., 1990, Geochemical evidence for Proterozoic continental arc and continental-margin rift magmatism along the northern margin of the Yangtze Craton, South China: Precambrian Research, v. 47, p. 205–221.

Gao, S., Qiu, Y., Ling, W., McNaughton, N.J., Zhang, B., Zhang, G., Zhang, Z., Zhong, Z., and Suo, S., 2002, SHRIMP single zircon U-Pb geochronology of eclogites from Yingshan and Xiongdian: Earth Science – Journal of China University of Geosciences, Wuhan, v. 27, p. 558–564.

Gilder, S.A., Leloup, P.H., Courtillot, V., Chen, Y., Coe, R.S., Zhao, X., Xiao, W., Halim, N., Cogné, J.-P., and Zhu, R., 1999, Tectonic evolution of the Tancheng-Lujiang (Tan-Lu) fault via Middle Triassic to Early Cenozoic paleomagnetic data: Journal Geophysical Research, v. 104, p. 15,365-15,390.

Graham, C., and Powell, R., 1984, A garnet-hornblende thermometer: calibration, testing, and application to the Pelona schists, southern California: Journal of Metamorphic Geology, v. 2, p. 13–31.

Green, D. and Hellmann, P., 1982, Fe-Mg partitioning between coexisting garnet and phengite at high pressures, and comments on a garnet-phengite thermometer: Lithos, v. 15, p. 253–266.

Grimmer, J.C., Jonckheere, R., Enkelmann, E., Ratschbacher, L., Hacker, B.R., Blythe, A., Wagner, G.A., Liu, S., Dong, S., 2002, Late Cretaceous–Tertiary history of the southern Tan-Lu fault zone: Apatite fission-track and structural constraints from the Dabie Shan: Tectonophysics, v. 359, p. 225-253.

Grimmer, J.C., Ratschbacher, L., Franz, L., Gaitzsch, I., Tichomirowa, M., McWilliams, M. O., Hacker, B.R., and Zhang, Y., 2003, When did the ultrahigh-pressure rocks reach the surface? A $^{207}Pb/^{206}Pb$ zircon, $^{40}Ar/^{39}Ar$ white mica, Si-in-phengite single grain study of Dabie Shan synorogenic foreland sediments: Chemical Geology, v. 197, p. 87–110.

Hacker, B.R., and Wang, Q., 1995, Ar/Ar geochronology of ultrahigh-pressure metamorphism in central China: Tectonics, v. 14, p. 994-1006.

Hacker, B.R., Wang, X., Eide, E.A., and Ratschbacher, L., 1996, Qinling–Dabie ultrahigh-pressure collisional orogen, *in* The Tectonic Evolution of Asia, Yin, A., and Harrison, T.M., eds.: Cambridge University Press, Cambridge, United Kingdom, p. 345-370.

Hacker, B.R., Modenfelder, J.L., and Gnos, E., 1996, Rapid emplacement of the Oman ophiolite: Thermal and geochronologic constraints: Tectonics, v. 15, p. 1230-1247.

Hacker, B.R., Ratschbacher, L., Webb, L., Ireland, T., Walker, D., and Dong, S., 1998, U/Pb zircon ages constrain the architecture of the ultrahigh-pressure Qinling-Dabie orogen, China: Earth and Planetary Science Letters, v. 161, p. 215–230.

Hacker, B.R., Ratschbacher, L., Webb, L., McWilliams, M., Calvert, A., Dong, S., Wenk, H. R., and Chateigner, D., 2000, Exhumation of the ultrahigh-pressure continental crust in east-central China: Late Triassic-Early Jurassic tectonic unroofing: Journal of Geophysical Research, v. 105, p. 13339–13364.

Hacker, B.R., Ratschbacher, L., and Liou, J.G., 2004, Subduction, collision and exhumation in the ultrahigh-pressure Qinling–Dabie orogen, *in* Malpas, J., Fletcher, C.J.N., Ali, J.R., and Aitchison, J.C., eds., Aspects of the Tectonic Evolution of China: Geological Society of London Special Publication 226, p. 157-175.

Hacker, B.R., Wallis, S., Ratschbacher, L., Grove, M., and Gehrels, G., 2005, U-Pb SIMS and LA-ICP-MS zircon and monazite ages constrain ultrahigh-pressure metamorphism and the architecture of the ultrahigh-pressure Sulu orogen: Earth and Planetary Science Letters, in press.

Harrison, T.M., Heizler, M.T., Lovera, O.M., Wenji, C., and Grove, M., 1994, A chlorine disinfectant for excess argon released from K-feldspar during step heating: Earth and Planetary Science Letters, v. 123, p. 95-104.

Hodges, H., and Spear, F., 1982, Thermometry, geobarometry at Mt. Moosilake, New Hampshire: American Mineralogist, v. 67, p. 1118–1134.

Holland, T.J.B., 1980, The reaction albite = jadeite + quartz determined experimentally in the range of 600-1200°C: American Mineralogist, v. 65, p. 129–134.

Holland, T.J.B., 1990, Activities of components in omphacite solid solutions: Contributions to Mineralogy and Petrology, v. 105, p. 446–453.

Holland, T.J.B., and Blundy, J., 1994, Non-ideal interactions in calcic amphiboles and their bearing on amphibole-plagioclase thermometry: Contributions to Mineralogy and Petrology, v. 116, p. 433–447.

Hu, N., Yang, J., An, S., and Hu, J., 1993, Metamorphism and tectonic evolution of the Shangdan fault zone, Shaanxi, China: Journal of Metamorphic Geology, v. 11, p. 537–548.

Jahn, B.-M., 1998, Geochemical and isotopic characteristics of UHP eclogites and ultramafic rocks in the Dabie orogen: Implications for continental subduction and collision tectonics: *in* Hacker, B.R., and Liou, J.G., eds., When continents collide: Geodynamics and Geochemistry of ultrahigh-pressure rocks, Kluwer Academic Publishers, p. 203-239.

Jahn, B.-M., Wu, F., Lo, Ch.-H., and Tsai, Ch.-H., 1999, Crust-mantle interaction induced by deep subduction of the continental crust: Geochemical and Sr-Nd isotopic evidence from post-collisional mafic-ultramafic intrusions of the northern Dabie complex, central China: Chemical Geology, v. 157, p. 119-146.

Jahn, B.-M.., Liu, X., Yui, T.-F., Morin, N, and Coz, M.B.-L., 2005, High-pressure/ultrahigh-pressure eclogites from the Hong'an Block, East-Central China: geochemical characterization, isotope disequilibrium and geochronological controversy: Contributions to Mineralogy Petrology, v. 149, p. 499-526.

Jian, P., Yang, W., Li, Z.C., and Zhou, H., 1997, Isotopic geochronological evidence for the Caledonian Xiongdian eclogite in the western Dabie mountains, China: Acta Geologica Sinica, v. 10, p. 455–465.

Jian, P., Liu, D., Yang, W., and Williams, I.S., 2001, SHRIMP dating of zircons from the Caledonian Xiongdian eclogite, western Dabie Mountains, China: Chinese Science Bulletin, v. 46, p. 77-79.

Jonckheere, R., 2003a, On the densities of etchable fission tracks in a mineral and co-irradiated external detector with reference to fission-track dating of minerals: Chemical Geology, v. 200, p. 41-58.

Jonckheere, R., 2003b, On the methodical problems in estimating geological temperature and time from measurements of fission tracks in apatite: Radiation Measurements, v. 36, p. 43-55.

Jonckheere, R., and Wagner, G.A., 2000, On the thermal stability of fossil and neutron-induced fission tracks in natural titanite: Nuclear Instruments and Methods in Physics Research, Section B, v. 168, p. 78-87.

Ketcham, R.A., Donelick, R.A., and Donelick, M.B., 2000, AFTSolve: A program for multikinetic modeling of apatite fission-track data: Geological Materials Research, v. 2, p. 1-32.

Kohn, M., and Spear, F., 1990, Two new geobarometers for garnet-amphibolites, with applications to southeastern Vermont: American Mineralogist, v. 75, p. 89–96.

Kretz, R., 1983, Symbols for rock-forming minerals: American Mineralogist, v. 68, p. 277–279.

Krogh, E., 2000, The garnet-clinopyroxene Fe/Mg thermometer: an updated calibration: Journal of Metamorphic Geology, v. 18, p. 211–219.

Kröner, A., Compston, W., Zhang, G. W., Guo, A. L., and Todt, W., 1988, Age and tectonic setting of late Archean greenstone-gneiss terrane in Henan province, China, as revealed by single-grain zircon dating: Geology, v. 16, p. 211–215.

Kröner, A., Zhang, G., and Sun, Y., 1993, Granulites in the Tongbai area, Qinling belt, China, geochemistry, petrology, single zircon geochronology, and implications for the tectonic evolution of eastern Asia: Tectonics, v. 12, p. 245–255.

Leake, B.E., Wooley, A. R., Arps, C., Birch, W., Gilbert, M., Grice, J., Hawthorne, F., Kato, A., Kisch, H., Krivovichev, V., Linthout, K., Mandarino, J. L. J., Maresch, V., Nickel, E., Rock, N., Schumacher, J., Smith, D., Stephenson, N., Ungaretti, L., Whittaker, E., and Youzhi, G., 1997, Nomenclature of amphiboles. Report of the subcommittee on amphiboles of the International Mineralogical Association Commission on new minerals and mineral names: European Journal of Mineralogy, v. 9, p. 623–665.

Laird, J., 1982, Amphiboles in metamorphosed basaltic rocks, Chapter 2: Reviews in Mineralogy, Mineralogical Society of America, p. 113–158.

Li, S.G., Hart, S.R., Zheng, S.G., Liu, D.L., Zhang, G.W., and Guo, A.L., 1989, Timing of collision between the north and south China blocks – The Sm-Nd isotopic age evidence: Science in China, v. 32, p. 1393–1400.

Li, S.G., Jagoutz, E., Zhang, Z.Q., Chen, W., and Lo, Q.H., 1995, Structure of high-pressure metamorphic belt in the Dabie mountains and its tectonic implications: Chinese Science Bulletin, v. 40, p. 138–140.

Li, S.G., Huang, F., Nie, Y.H., Han, W.L., Long, G., Li, H.M., Zhang, S.Q., and Zhang, Z.-H., 2001, Geochemical and geochronological constraints on the suture location between the North and South China blocks in the Dabie Orogen, Central China: Physics and Chemistry of the Earth, Part A: Solid Earth and Geodesy, v. 26, p. 655–672.

Li, X.H., 1999, U-Pb zircon ages of granites from the southern margin of the Yangtze Block: timing of Neoproterozoic Jinning orogeny in SE China and implications for Rodinia assembly: Precambrian Research, v. 97, p. 43–57.

Li, Z.X., Zhang, L., and Powell, McA., Ch., 1995, South China in Rodinia: Part of the missing link between Australia-East Antarctica and Laurentia?: Geology, v. 23, p. 407–410.

Li, Z.X., Li, X.H., Kinny, P.D., and Wang, J., 1999, The break-up of Rodinia: did it start with a mantle plume beneath South China?: Earth and Planetary Science Letters, v. 173, p. 171–181.

Li, Z.X., Li, X.H., Zhou, H., and Kinny, P.D., 2002, Grenvillian continental collision in south China: New SHRIMP U-Pb zircon results and implications for the configuration of Rodinia: Geology, v. 30, p. 163–166.

Lin, W., Faure, M., Monié, P., Schärer, U., Zhang, L., and Sun, Y., 2000, Tectonics of SE China: New insights from the Lushan massif (Jiangxi Province): Tectonics, v. 19, p. 852–871.

Liou, J.G., Zhang, R.Y., Eide, E.A., Maruyama, S., Wang, X., and Ernst, W.G., 1996, Metamorphism and tectonics of high-P and ultrahigh-P belts in Dabie-Sulu Regions, eastern central China, *in* Yin, A. and Harrison T.M., eds., The Tectonic Evolution of Asia: Cambridge University Press, Cambridge, United Kingdom, p. 300–343.

Liu, Y.-C., Li, S.-G., Xu, S.-T., Jahn, B.-M., Zheng, Y.-F., Zhang, Z.-Q., Jiang, L.-L., Chen, G.-B., and Wu, W.-P., 2001, Sm-Nd dating of eclogites from North Dabie and its constraints on the timing of granulite-facies retrogression: Geochimica, v. 30, p. 79–87.

Liu, D., Tang, J., Zhou, Ch., Gao, T., Shen, H., and Yang, Ch., 2002, U-Pb zircon dating and its geological significance of the Taoyuanzhai volcanic rocks, Central Dabie orogenic belt: Acta Geologica Sinicia, v. 76, p. 217–221.

Liu, X., Jahn, B.-M., Liu, D., Dong, S., and Li, S., 2004a, SHRIMP U–Pb zircon dating of a metagabbro and eclogites from western Dabieshan (Hong'an Block), China, and its tectonic implications: Tectonophysics, v. 394, p. 171–192.

Liu, X., Wei, C., Liu, S., Dong, S., and Liu, J., 2004b, Thermobaric structure of a traverse across western Dabieshan: implications for collision tectonics between the Sino-Korean and Yangtze cratons: Journal metamorphic Geology, v. 22, p. 361–379.

Lovera, O.M., Grove, M., Harrison, T.M., and Mahon, K.I., 1997, Systematic analysis of K-feldspar $^{40}Ar/^{39}Ar$ step heating results; I, Significance of activation energy determinations: Geochimica et Cosmochimica Acta, v. 61, p. 3171-3192.

Maresch, W., 1977, Experimental studies on glaucophane: an analysis of present knowledge: Tectonophysics, v. 43, p. 109-125.

Maryuama, S., Cho, M., and Liou, J., 1986, Experimental investigations of greenschist-blueschist transition equilibria: Pressure dependence of Al contents in sodic amphiboles. A new geobarometer: Geological Society of America Memoir, v. 164, p. 1–16.

Massonne, H., and Schreyer, W., 1987, Phengite barometry based on the limiting assemblage with K-feldspar, phlogopite and quartz: Contributions to Mineralogy and Petrology, v. 96, p. 212–224.

Massonne, H., and Szpurka, Z., 1997, Thermodynamic properties of white micas on the basis of high-pressure experiments in the system K_2O-MgO-Al_2O_3-SiO_2-H_2O and K_2O-FeO-Al_2O_3-SiO_2-H_2O: Lithos, v. 41, p. 229–250.

Mattauer, M., Matte, P., Malavieille, J., Tapponnier, P., Maluski, H., Xu, Z.Q., Lu, Y.L., and Tang, Y.Q., 1985, Tectonics of the Qinling belt: Build-up and evolution of eastern Asia: Nature, v. 317, p. 496-500.

Mattauer, M., Matte, Ph., Maluski, H., Xu, Z., Zhang Q., and Wang, Y.-M., 1991, La limite Chine du Nord-Chine du Sud au Paleozoique et au Trias. Nouvelles donnees structurales et radiometriques dans le massif de Dabie-Shan (chaine des Qinling): Compte Rendu Academie Science, Paris, v. t. 312, p. 1227-1233.

Niu, B., Liu, Z., and Ren, J., 1993, The tectonic relationship between the Qinling Mountains and Tongbai-Dabie Mountains with notes on the tectonic evolution of the Hehuai Basin: Bulletin of the Chinese Academy of Geological Sciences, v. 26, p. 1-12.

Niu, B., Fu, Y., Liu, Z., Ren, J., and Chen, W., 1994, Main tectonothermal events and $^{40}Ar/^{39}Ar$ dating of the Tongbai–Dabie Mts.: Acta Geoscientia Sinica, v. 1994, p. 20–34.

Oberhänsli, R., Martinotti, G., Schmid, R., and Liu, X., 2002, Preservation of primary volcanic textures in the ultrahigh-pressure terrain of Dabie Shan: Geology, v. 30, p. 699–702.

Okay, A., Sengör, A., and Satir, M., 1993, Tectonics of an ultrahigh-pressure metamorphic terrane: Dabie Shan, China: Tectonics, v. 12, p. 1320–1334.

Papike, J.J., Cameron K.L., and Baldwin, K., 1974, Characterization of other than quadrilateral components and estimates of ferric iron from microprobe data: Geological Society of America, Abstract with Programs, v. 6, p. 1053-1054.

Passaglia, E., and Gotthardi, G., 1973, Crystal chemistry and nomenclature of pumpellyites and jugoldites: Canadian Mineralogists, v. 12, p. 219–223.

Passchier, C., and Trouw, R., 1996, Microtectonics: Springer-Verlag, Berlin, pp. 289.

Ratschbacher, L., Hacker, B., Webb, L., McWilliams, M., Ireland, T., Dong, S., Calvert, A., Chateigner, D., and Wenk, H. R., 2000, Exhumation of the ultrahigh-pressure continental crust in east-central China: Cretaceous and Cenozoic unroofing and the Tan-Lu fault: Journal of Geophysical Research, v. 105, p. 13303–13338.

Ratschbacher, L., Hacker, B.R., Calvert, A., Webb, L.E., Grimmer, J.C., McWilliams, M.O., Ireland, T.R., Dong, S., and Hu, J., 2003, Tectonics of the Qinling (central China): Tectonostratigraphy, geochronology, and deformation history: Tectonophysics, v. 366, p. 1–53.

Reiners, P.W., Zhou, Z., Ehlers, T.A., Xu, C., Brandon, M.T., Donelick, R.A., and Nicolescu, S., 2003, Post-orogenic evolution of the Dabie Shan, eastern China, from (U-Th)/He and fission-track thermochronology: American Journal of Science, v. 303, p. 489-518.

Ren, J., Tamaki, K., Li, S., and Junxia, Z., 2002, Late Mesozoic and Cenozoic rifting and its dynamic setting in Eastern China and adjacent areas: Tectonophysics, v. 344, p. 175-205.

R.G.S. Henan, 1989, Regional Geology of Henan Province (in Chinese): Geological Publishing House, Beijing.

R.G.S. Sichuan, 1991, Regional Geology of Sichuan Province, (in Chinese): Geological Publishing House, Beijing.

R.G.S. Shaanxi, 1989, Regional Geology of Shaanxi Province, (in Chinese): Geological Publishing House, Beijing.

Rowley, D.B., and F. Xue, 1996, Modeling the exhumation of ultra-high pressure metamorphic assemblages; observations from the Dabie/Tongbai region, China: Geological Society of America Abstracts with Programs, v. 28, p. 249.

Ryburn, R., Rahem, A., and Green, D., 1976, Determination of the PT-path of natural eclogites during metamorphism - record of a subduction: Lithos, v. 9, p. 161–164.

Schmid, R., Franz, L., Oberhänsli, R., and Dong, S., 2000, High Si-phengite, mineral chemistry and P-T evolution of ultra-high-pressure eclogites and calc-silicates from the Dabie Shan, eastern PR China: Geological Journal, v. 35, p. 185-207.

Schmid, R., Wilke, M., Oberhänsli, R., Janssens, K., Falkenberg, G., Franz L., and Gaab, A., 2003, Micro-XANES determination of ferric iron and its application in thermobarometry: Lithos, v. 70, p. 381-392.

Schliestedt, M., 1980, Phasengleichgewichte in Hochdruckgesteinen von Sifnos, Griechenland: Ph.D. thesis, TU Braunschweig.

Sun, W., Williams, I.S., and Li, S., 2002, Carboniferous and Triassic eclogites in the western Dabie Mountains, east-central China: evidence for protracted convergence of the North and South China Blocks: Journal of Metamorphic Geology, v. 20, p. 873–886.

Suo, S.T., Sang, L., Han, Y., You, Z., and Zhou, N., 1993, The petrology and tectonics in Dabie Precambrian metamorphic terrane, central China: Press of the China University of Geosciences, Wuhan, p. 33-112.

Terebayashi, M., 1988, Actinolite-forming reactions at low pressure and the role of the Fe^{2+}-Mg substitution: Contribution to Mineralogy and Petrology, v. 100, p. 268–280.

Triboulet, C., Thieblemont, D., and Audren, C., 1992, The (Na-Ca) amphibole-albite-chlorite-epidote-quartz thermobarometer in the system S-A-F-M-C-N-H_2O: An empirical calibration: Contributions to Mineralogy and Petrology, v. 10, p. 545–556.

Twiss, R.J., and Unruh, J.R., 1998, Analysis of fault slip inversions: Do they constrain stress or strain rate?: Journal Geophysical Research, v. 103, p. 12205–12221.

Wallis, S., Enami, M., and Banno, S., 1999, The Sulu UHP Terrane: A review of the petrology and structural geology: International Geology Review, v. 41, p. 906-920.

Wan, Y., Li, R., Wilde, S.A., Liu, D., Chen, Z., Yan, L., Song, T., and Yin, X., 2005, UHP metamorphism and exhumation of the Dabie Orogen, China: Evidence from SHRIMP dating of zircon and monazite from a UHP granitic gneiss cobble from the Hefei Basin: Geochimica et Cosmochimica Acta, in press.

Wang Q., Lia, R., Wang, D., and Li, S., 2003, Eclogites preserved as pebbles in Jurassic conglomerate, Dabie Mountains, China: Lithos v. 70, p. 345– 357.

Wang, X., and Liou, J., 1993, Regional ultrahigh-pressure coesite-bearing eclogitic terrane in central China: Evidence from country rock, gneiss, marble and metapelite: Journal of metamorphic Geology, v. 11, p. 575–588.

Waters, D., and Martin, H., 1993, Geobarometry of phengite-bearing eclogites (updated calibration of 1996 at: www.earth.ox.ac.uk/davewa/ecbar.html): Terra Abstracts, v. 5, p. 410–411

Webb, L., Hacker, B.R., Ratschbacher, L., and Dong, S.W., 1996, Structures and kinematics of exhumation: Ultrahigh-pressure rocks in the Hong'an block of the Qinling–Dabie ultrahigh-pressure orogen, E. China: Geological Society of America Abstracts with Programs, v. 27, p. 69.

Webb, L.E., Hacker, B.,R., Ratschbacher, L., McWilliams, M., and Dong, S., 1999, Thermochronologic constraints on deformation and cooling history of high and ultrahigh-pressure rocks in Qinling-Dabie orogen, eastern China: Tectonics, v. 18, p. 621–638.

Webb, L. E., Ratschbacher, L., Hacker, B.R., and Dong, S., 2001, Kinematics of exhumation of high- and ultrahigh-pressure rocks in the Hong'an and Tongbai Shan of the Qinling–Dabie collisional orogen, eastern China, *in* Hendrix, M. S. and

Davis, G. A., eds., Paleozoic and Mesozoic tectonic evolution of central Asia from continental assembly to intracontinental deformation: Geological Society of America Special Paper, v. 194, p. 231–245.

Wu, F.-Y., Lin, J.-Q., Wilde, S.A., Zhang X. and Yang, J.-H., 2005, Nature and significance of the Early Cretaceous giant igneous event in eastern China: Earth and Planetary Science Letters, v. 233, p. 103-119.

Xie, Z., Chen, J.-P., Zhou, T.-X., Li, H.-M., Zao, Y.-C., and Zhou, H.-Y., 1998, U-Pb zircon ages of the rocks in the North Dabie Terrain, China: Scientia Geologica Sinica, v. 7, p. 501-511.

Xie, Z., Chen, J.-F., Zhang, X., Gao, T.-S., Dai, Z.-Q., Zhou, T.-X., and Li, H.-M., 2001, Zircon U-Pb dating of gneiss from Shizhuhe in North Dabie and its geological implications: Acta Petrologica Sinica, v. 17, p. 139-144.

Xie, Z., Zheng, Y.-F., Jahn, B.-M., Ballevre, M., Chen, J., Gautier, P., Gao, T., Gong, B., and Zhou, J., 2004, Sm-Nd and Rb-Sr dating of pyroxene–garnetite from North Dabie in east-central China: problem of isotope disequilibrium due to retrograde metamorphism: Chemical Geology, v. 206, p. 137-158.

Xu, S.T., Jiang, L., Liu, Y., and Zhang, Y., 1992, Tectonic framework and evolution of the Dabie orogen in Anhui, eastern China, Acta Geologica Sinica, v. 66, p. 1-14.

Xu, B., Grove, M., Wang, Ch., Zhang, L., and Liu, S., 2000, $^{40}Ar/^{39}Ar$ thermochronology from the northwestern Dabie Shan: constraints on the evolution of Qinling–Dabie orogenic belt, east-central China: Tectonophysics, v. 322, p. 279-301.

Xu Ch., Zhou, Z., Van Den Haute, P., Donelick, R.A., De Grave, J., Changqian M.A., and Reiners, P.W., 2005, Apatite fission track geochronology and its tectonic correlation in the Dabieshan orogen, Central China: Science in China, Series D, v. 48, p. 506-520.

Xue, F., Lerch, F., Kröner, A., and Reischmann, T., 1996, Tectonic evolution of the East Qinling Mountains, China, in the Paleozoic: a review and a new tectonic model: Tectonophysics, v. 253, p. 271–284.

Xue, F., Rowley, D.B., Tucker, R.D., and Peng, Z.X., 1997, U-Pb zircon ages of granitoid rocks in the north Dabie complex, eastern Dabie Shan, China: Journal of Geology, v. 105, p. 744–753.

Yang, J.S., Liu, F.L., Wu, C.L., Xu, Z.Q., Shi, R.D., Chen, S.Y., Deloule, E., and Wooden, J.L., 2005, Two ultrahigh-pressure metamorphic events recognized in the central orogenic belt of China: Evidence from the U-Pb dating of coesite-bearing zircons: International Geology Review, v. 47, p. 327-343.

Ye, B.D., Jiang, P., Xu, J., Cui, F., Li, Z., and Zhang, Z., 1993, The Sujiahe terrane collage belt and its constitution and evolution along the northern hillslope of the Tongbai–Dabie orogenic belt: Press of China University of Geoscience, Wuhan, p. 66-67.

Ye, B.D., Jiang, P., Xu, J., Cui, F., Li, Z., and Zhang, Z., 1994, Timing of the Sujiahe group in the Tongbai–Dabie orogenic belt, *in* Chen, H., ed., Research of Isotope Geochemistry: Zhejiang University Press, Hangzhou, p. 175-186.

Yu, Z., and Meng, Q., 1995, Late Paleozoic sedimentary and tectonic evolution of the Shangdan suture zone, eastern Qinling, China: Journal of Southeast Asian Earth Sciences, v. 11, p. 237-242.

Zhai, X., Day, H.W, Hacker, B.R, and You, Z., 1998, Paleozoic metamorphism in the Qinling orogen, Tongbai mountains, central China: Geology, v. 26, p. 371–374.

Zhang, K.-J., 1997, North and South China collision along the eastern and southern North China margins: Tectonophysics, v. 270, p. 145-156.

Zhang, D., and Sun, G., 1990, Emplacement age of the Tiantangzhai granite massif, Dabie Mountains and its geological significance: Acta Petrologica Mineralogica, v. 6, p. 31.

Zhang, R., and Liou, J.G., 1994, Coesite-bearing eclogite in Henan Province, central China: detailed petrography, glaucophane stability and PT-path: European Journal of Mineralogy, v. 6, p. 217–233.

Zhang, Y.Q., Vergely, P., and Mercier, J.L., 1995, Active faulting in and along the Qinling Range (China) inferred from SPOT imagery analysis and extrusion tectonics of southern China: Tectonophysics, v. 243, p. 69-95.

Zhao, X., and Coe, R.S., 1987, Paleomagnetic constraints on the collision and rotation of North and South China: Nature, v. 327, p. 141-144.

Zhong, Z., Suo, S., and You, Z., 1999, Regional-scale extensional tectonic pattern of ultrahigh-P and high-P metamorphic belts from the Dabie massif, China: International Geologic Review, v. 41, p. 1033–1041.

Zhong, Z., Suo, S., You, Z., Zhang, H., and Zhou, H., 2001, Major constituents of the Dabie collisional orogenic belt and partial melting in the ultrahigh-pressure unit: International Geologic Review, v. 43, p. 226–236.

Zhou, T., Chen, J., Li, X., and Foland, K.A., 1992, $^{40}Ar/^{39}Ar$ isotope dating of intrusions from Huoshan–Shucheng syenite zone: Anhui Geology, v. 2, p. 4–11.

Zhou, G., Liu, J., Eide, E., Liou, J.G., and Ernst, W.G., 1993, High pressure/low temperature metamorphism in northern Hubei province, central China: Journal of Metamorphic Geology, v. 11, p. 561–574.

Zhou, M.-F., Yan, D.-P., Kennedy, A.K., Li, Y., and Ding, J., 2002, SHRIMP U-Pb zircon geochronological and geochemical evidence for Neoproterozoic arc-magmatism along the western margin of the Yangtze block, South China: Earth and Planetary Science Letters, v. 196, p. 51-67.

Zhou, Z., Xu, C., Reiner, P.W., Yang, F., and Donelik, R.A., 2003, Late Cretaceous–Cenozoic exhumation history of Tiantangzhai region of Dabieshan orogen: constraints from (U-Th)/He and fission-track analysis: Chinese Science Bulletin, v. 48, p. 1151–1156.

FIGURE CAPTIONS

Figure 1: The Qilian–Qinling–Tongbai–Hong'an–Xinxian–Dabie–Sulu–Imjingang collisional orogen of eastern Asia. Structural interpretations of Triassic sub-horizontal extension in crystalline basement domes from Faure et al. (1996, 2003), Wallis et al. (1999), Lin et al. (2000), Hacker et al. (2000), and Ratschbacher et al. (2003). Andesitic volcanic rocks from Zhang (1997) and Permian–Triassic plutons from R.G.S. Sichuan (1991) and R.G.S. Shaanxi (1989).

Figure 2: Correlation of geological units of the northern margin of Tongbai–Xinxian–Dabie orogenic belt, distribution of Early Cretaceous plutons, and reliable geochronological ages: ★, location; red, pre-Cretaceous; green, Cretaceous; orange, station with new petrology (sample number and, if applicable, age in bold). Geochronological references: *, this paper (sample number and age in bold); 1, Kröner et al. (1993); 2, R.G.S Henan (1989); 3, Ye et al. (1993); 4, Li et al. (2001); 5, Chen et al. (2003); 6, Hacker et al. (2000); 7, Zhai et al. (1988); 8, Li et al. (1989); 9, Jian et al. (1997); 10, Jian et al. (2001); 11, Sun et al. (2002); 12, Xie et al. (2001) ; 13, Niu et al. (1994); 14, Liu et al. (2002) ; 15, Liu et al. (2001); 16, Chen et al. (1998); 17, Hacker et al. (1998); 18, Eide et al. (1994); 19, Liu et al. (2004a); 20, Gao et al. (2002); 21, Liu et al. (1995); 22, Xu et al. (2000); 23, Webb et al. (1999); 24, Xie et al. (2004); 25, Zhou et al. (1992); 26, Xie et al. (1998); 27, Ratschbacher et al. (2000); 28, Hacker and Wang (1995); 29, Xue et al. (1997); 30, Mattauer et al. (1991); 31, Zhang and Sun (1990); 32, Chen et al. (1995); 33, Jahn et al. (1999); 34, Jahn et al. (2005). Ages of Niu et al. (1994) were recalculated; they may deviate from those given in the original publication. Abbreviations for geochronology: Z, U/Pb zircon; H, $^{40}Ar/^{39}Ar$ hornblende; K/Ar, potassium-

argon on undefined mineral; B, $^{40}Ar/^{39}Ar$ biotite; M, $^{40}Ar/^{39}Ar$ muscovite; K, $^{40}Ar/^{39}Ar$ K-feldspar; Rm, Rb/Sr muscovite, Rwr, Rb/Sr, whole rocks; Swr, Sm/Nd, whole rock.

Figure 3: Histograms and relative frequencies of reliable ages from the Qinling–Tongbai–Xinxian–Dabie belt used for regional correlations and definition of tectonothermal events. S data and discussion in text, Fig. 2, Tables 1–2, and Table 12; the latter is at http://www.geol.tu-freiberg.de/tectono/E_Links.htm.

Figure 4: New $^{40}Ar/^{39}Ar$ data. See Table 1 for sample location, age data, and interpretations. Weighted mean ages (WMA) were calculated using shaded steps. TFA, total fusion age; IA, isochron age. Uncertainties are 1σ except where noted. Diffusion-domain analysis of metamorphic K-feldspars shows Arrhenius plot, log(R/R_0) plot, release spectrum, and range of cooling histories.

Figure 5: Simplified map of Cretaceous (a) and Cenozoic (b) structures in Tongbai–Xinxian and Cenozoic structures in northern Dabie (c). Maps modified from and unlabeled data taken from Ratschbacher et al. (2000). Lower hemisphere, equal-area stereograms show ductile and brittle structural data: sf, foliation; str, mineral stretching lineation; sb, shear band. Fault-slip data and principal stress orientations 1–3: Faults are drawn as great circles and striae are drawn as arrows pointing in the direction of displacement of the hanging wall. Confidence levels of slip-sense determination are expressed in the arrowhead style: solid, certain; open, reliable; half, unreliable; without head, poor. Arrows around the plots give calculated local orientation of sub-horizontal principal compression and tension. Inset in (a) gives schematic NE–SW profile across the Tongbai–Xinxian with location of major faults, Cretaceous plutonism, and apatite fission-track ages. In (b) apatite (A) and titanite (T) fission-track data are plotted together with reliable data from the literature (Grimmer et al., 2002; Reiners et al., 2003; Zhou et al., 2003; Xu et al., 2005). Insets in (a)–(c): Fission-track length distributions and T[t]-paths of representative samples. In T[t]-path diagrams the arrow at the top of each diagram indicates the range of initial constraints for which the depicted T[t]-path solutions are valid. The constraints are represented by the bold vertical lines. The vertical line with the number at the bottom of each diagram gives the apatite fission-track age in Ma.

Figure 6. (a) Pressure–temperature–time (PTt) path for the Huwan shear-zone rocks straddling the Xinxian complex, the Huwan mélange, and the Dingyuan complex. PT estimates with

error bars are for the Late Paleozoic Xiongdian eclogitic metabasites (squares), Triassic Xinxian eclogite (diamond), and Early Paleozoic Dingyuan greenschist (circle; core and rim sections). Amphibole out after Carswell (1990), glaucophane in after Maresch (1977), quartz–coesite transition after Bohlen and Boetcher (1982). (b) PTt data of the Guishan complex with hypothetical PTt path; error bars indicate the spread of the analytical data. (c) Prograde, clockwise PT loop for Erlangping amphibole schist. Error due to Fe^{3+}-estimate indicated by cross bar.

Figure 7: As Figure 5 but for Triassic and Silurian–Devonian structural data. B, fold axis ($_1$, first generation; $_2$, second generation); sz, shear zone; tg, tension gash; s_0, bedding; shear sense from asymmetric boudinage (ab), sigma-clasts (σ), calcite texture (cc), quartz texture (qtz), shear zones (sz). G, Guishan complex; D, Dingyuan complex; C, Carboniferous metaclastic rocks. Stress-analysis parameters (below fault-slip data figures): see Ratschbacher et al. (2000) for explanation and methodology. Letter and numbers at the lower right of some stereogram give mineral and age of geochronology measured at this station.

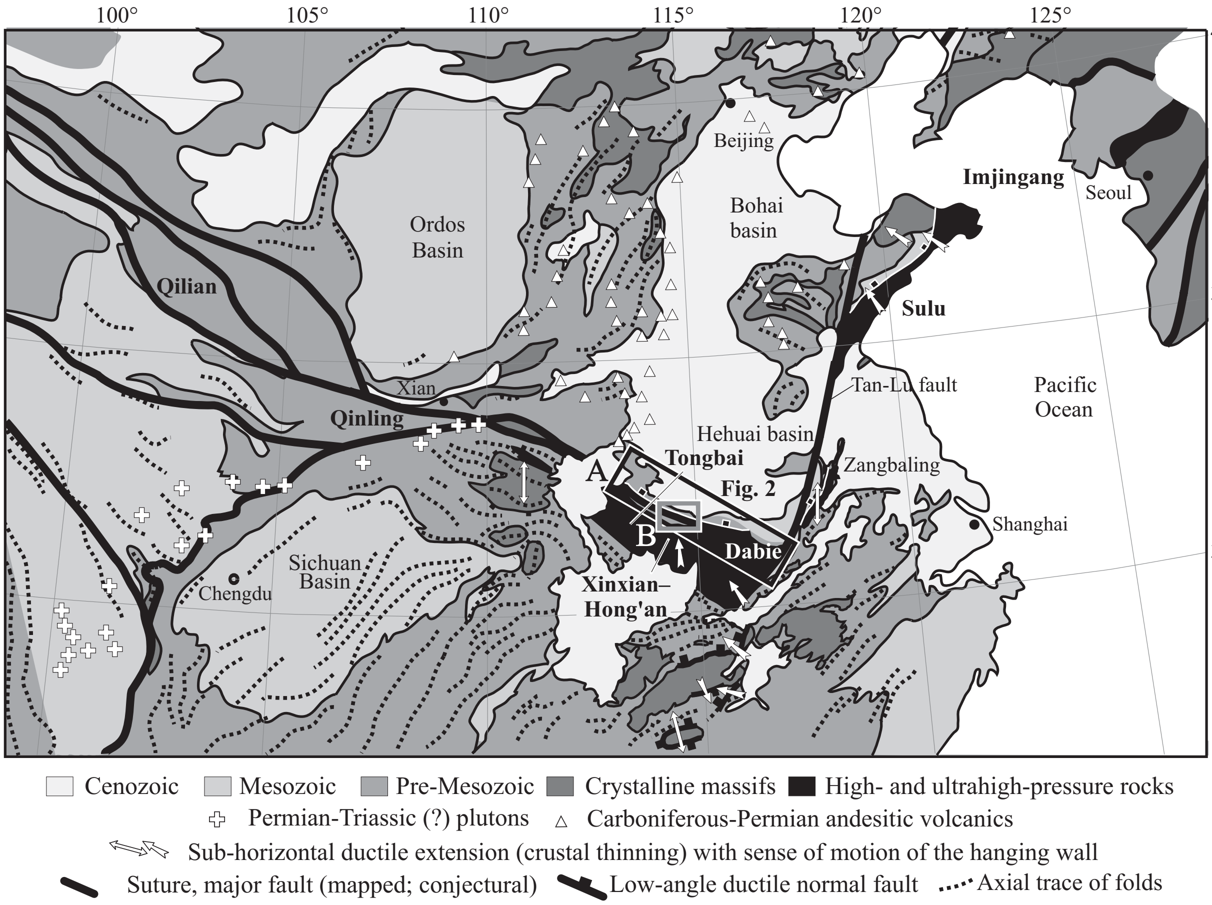

Figure 1: Ratschbacher et al.

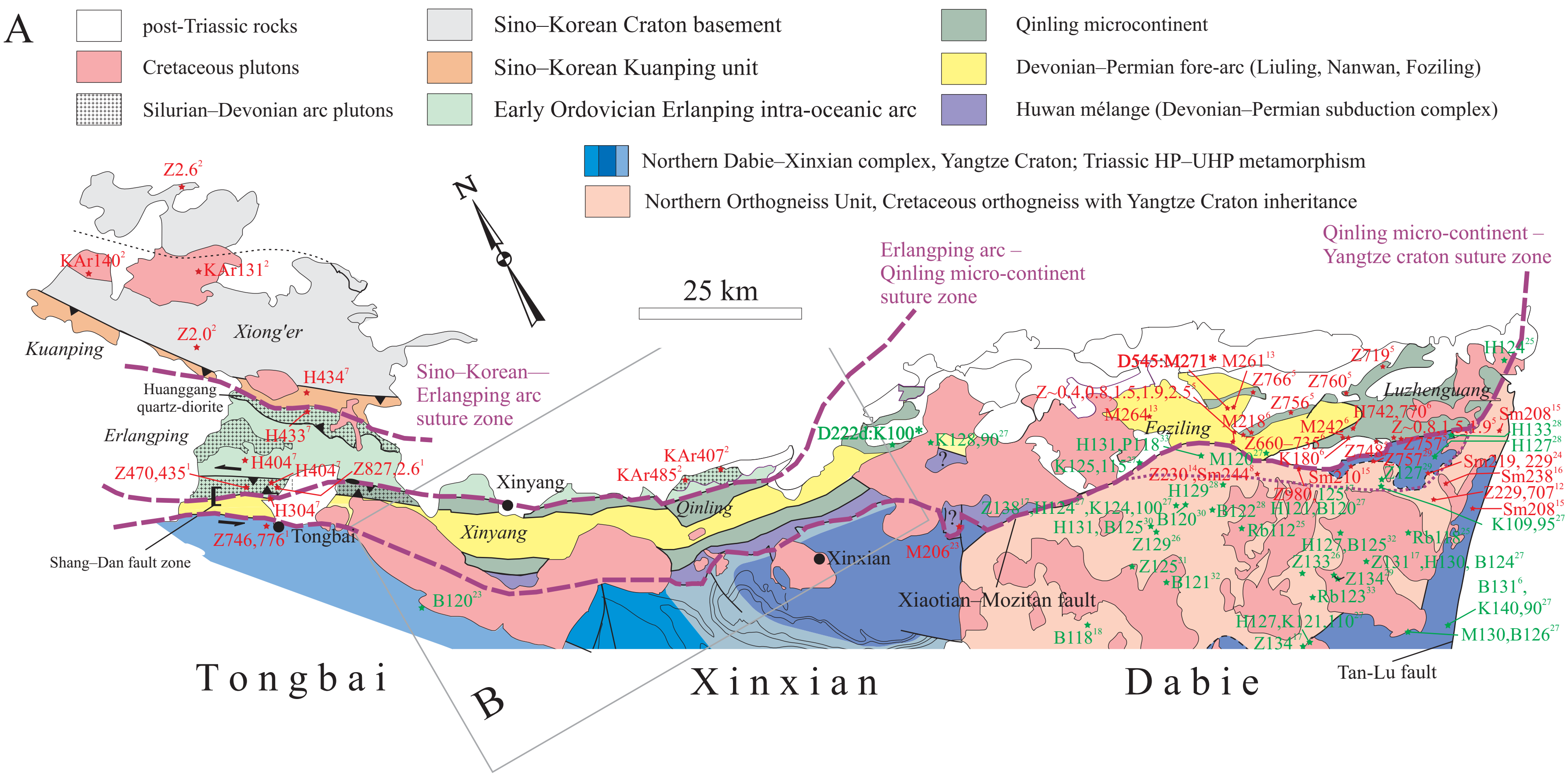

Figure 2a: Ratschbacher et al.

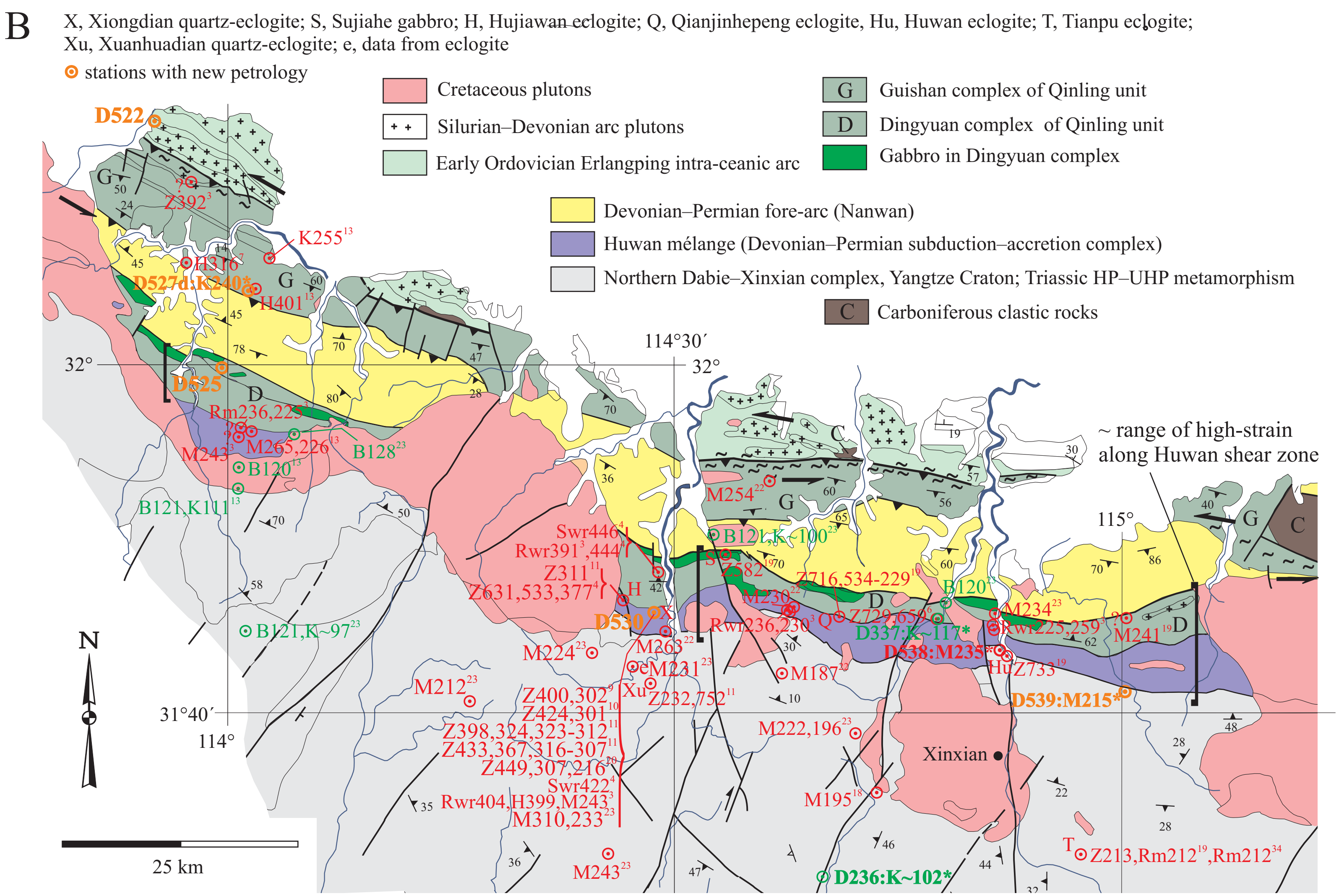

Figure 2b: Ratschbacher et al.

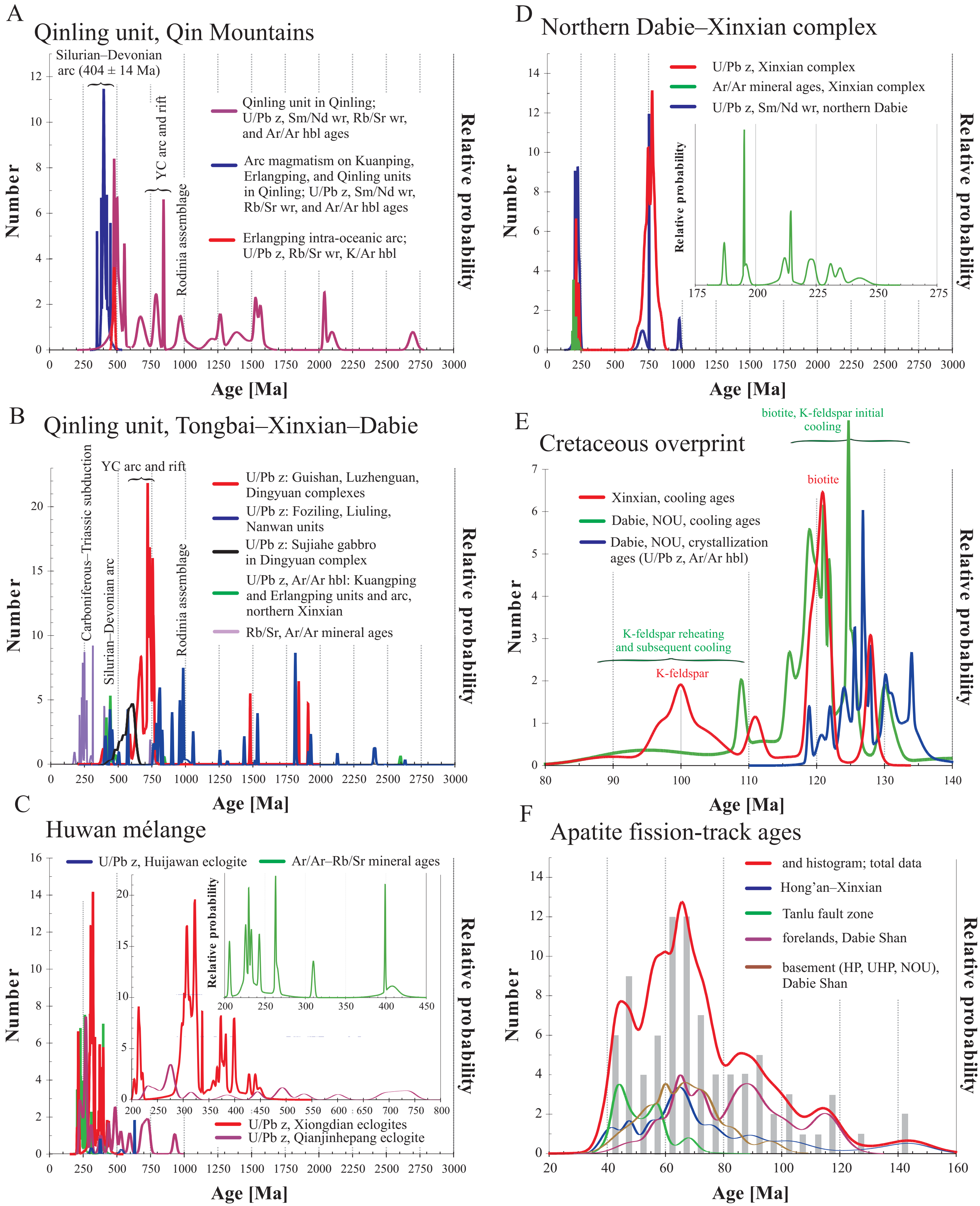

z, zircon; wr, whole-rock; hbl, hornblende; NOU, Northern Orthogneiss Unit of northern Dabie Shan

Figure 3, Ratschbacher et al.

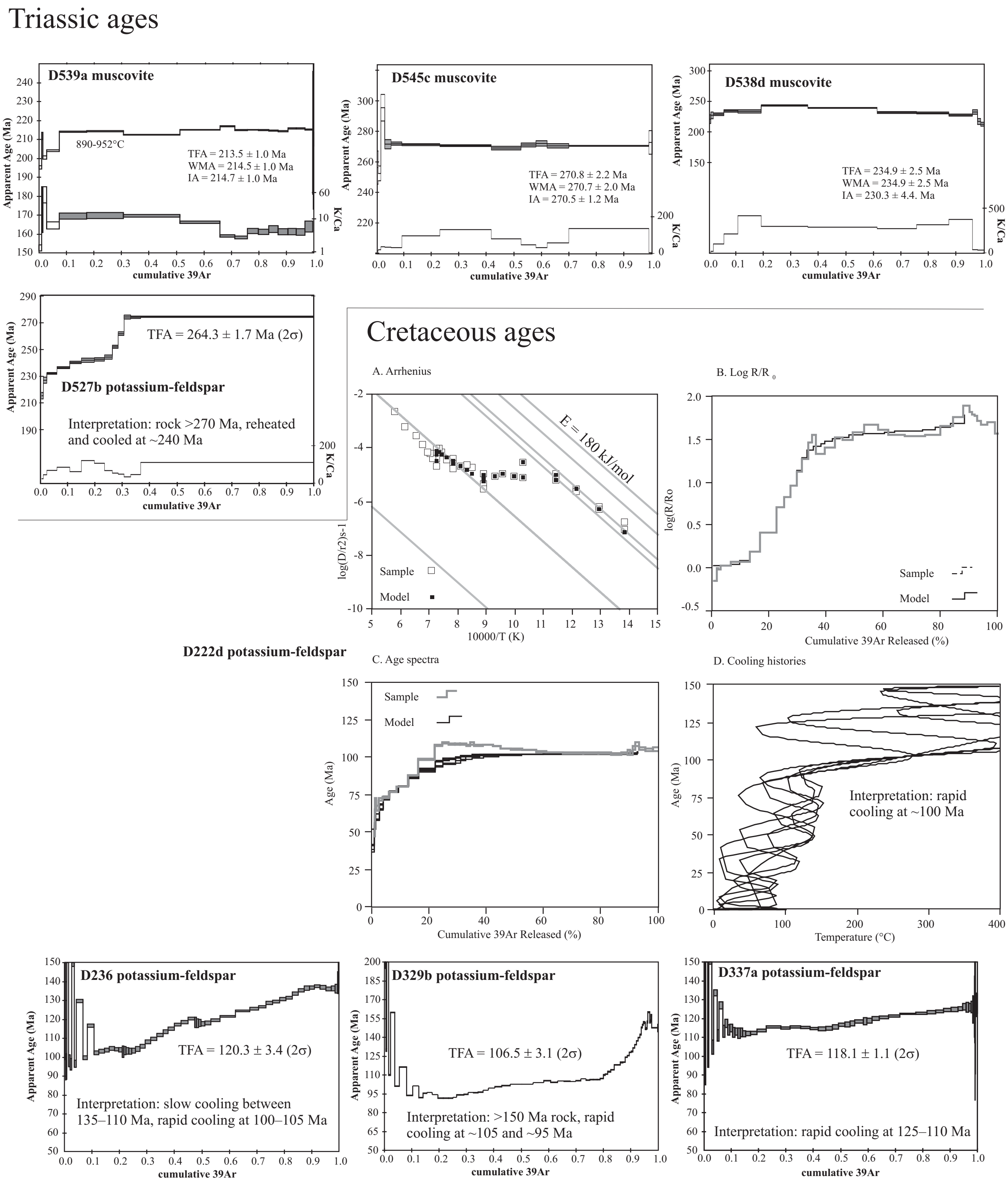

Figure 4, Ratschbacher et al.

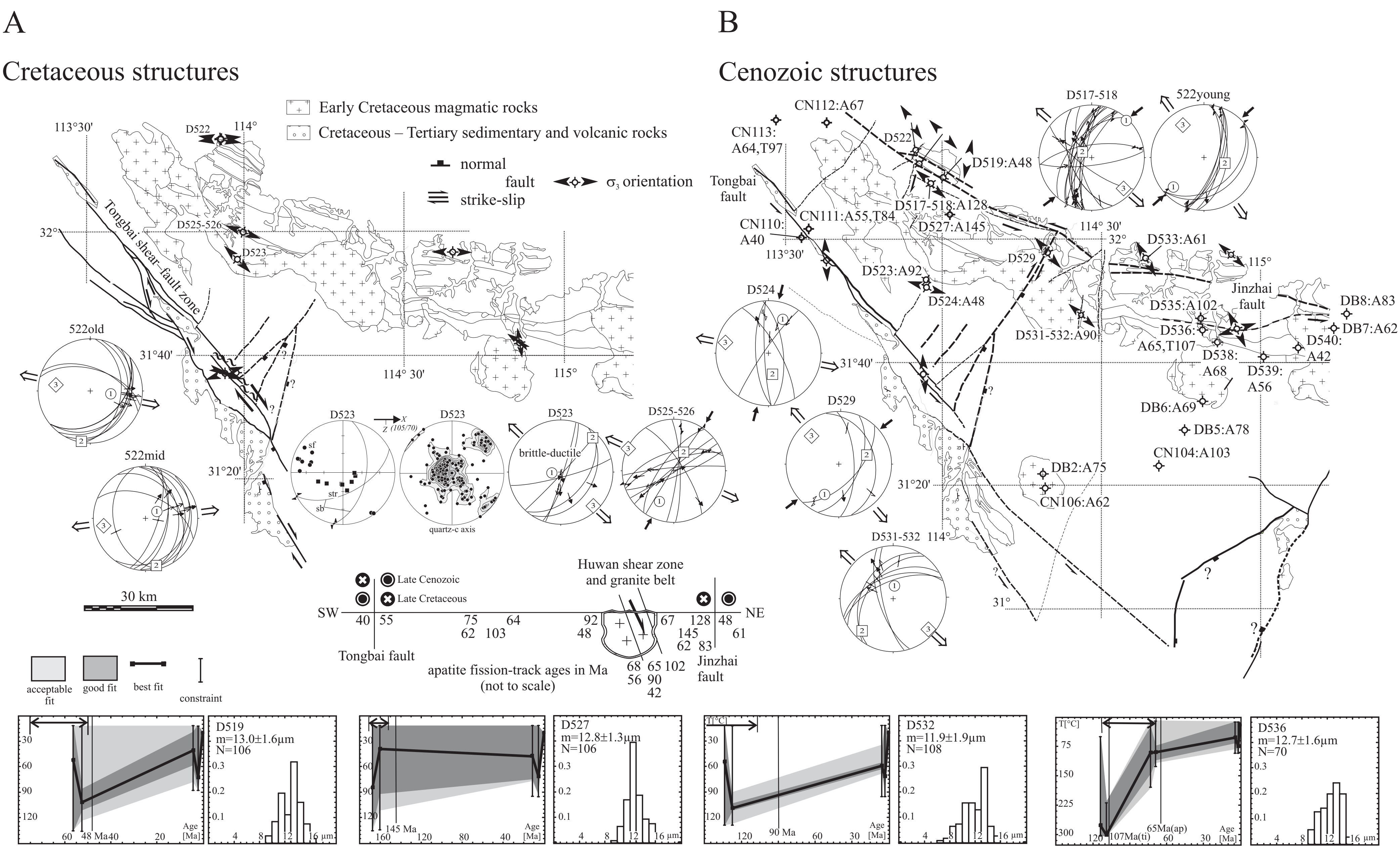

Figure 5a,b, Ratschbacher et al.

C

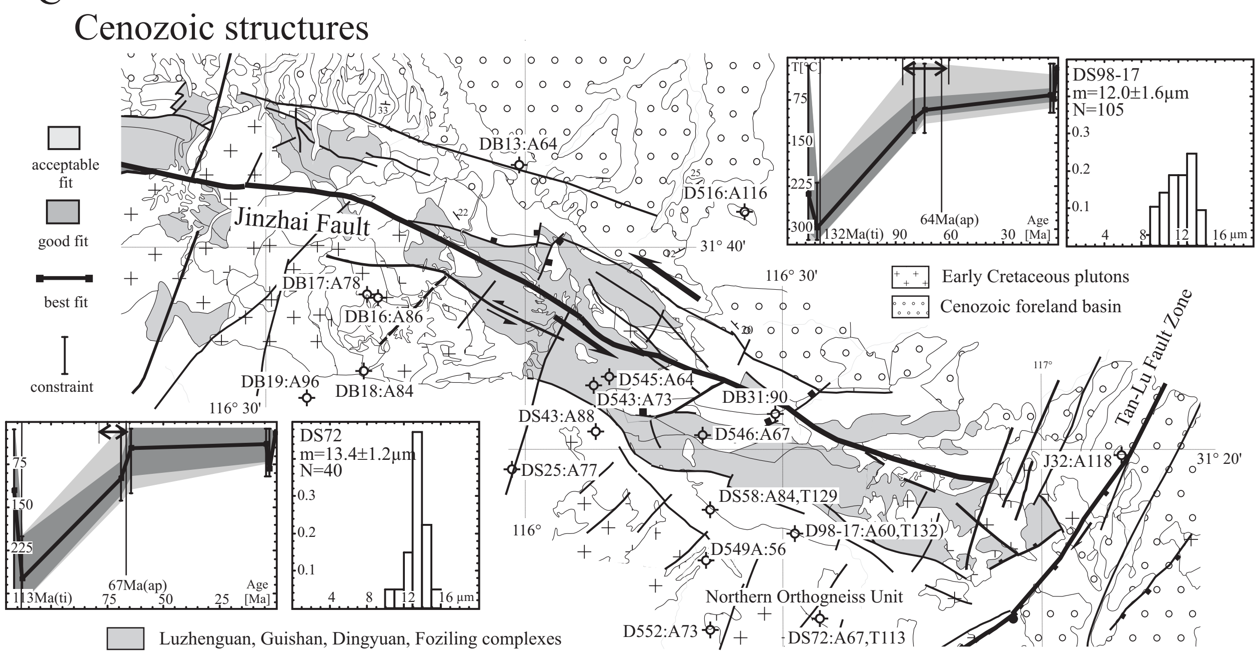

Figure 5c, Ratschbacher et al.

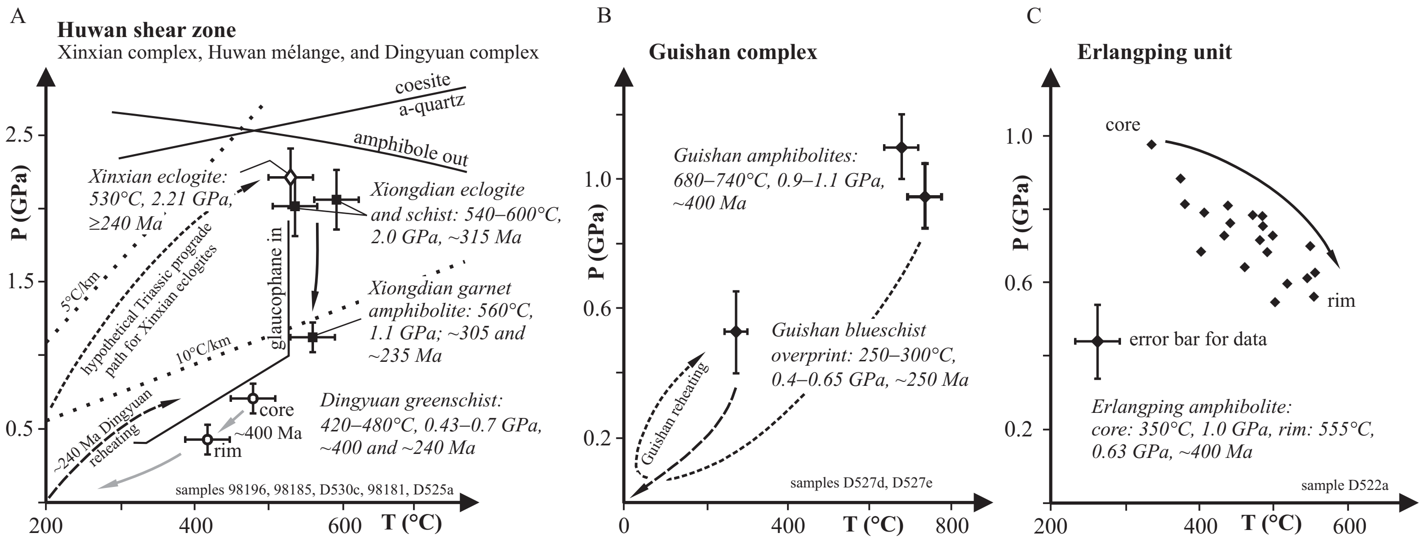

Figure 6, Ratschbacher et al.

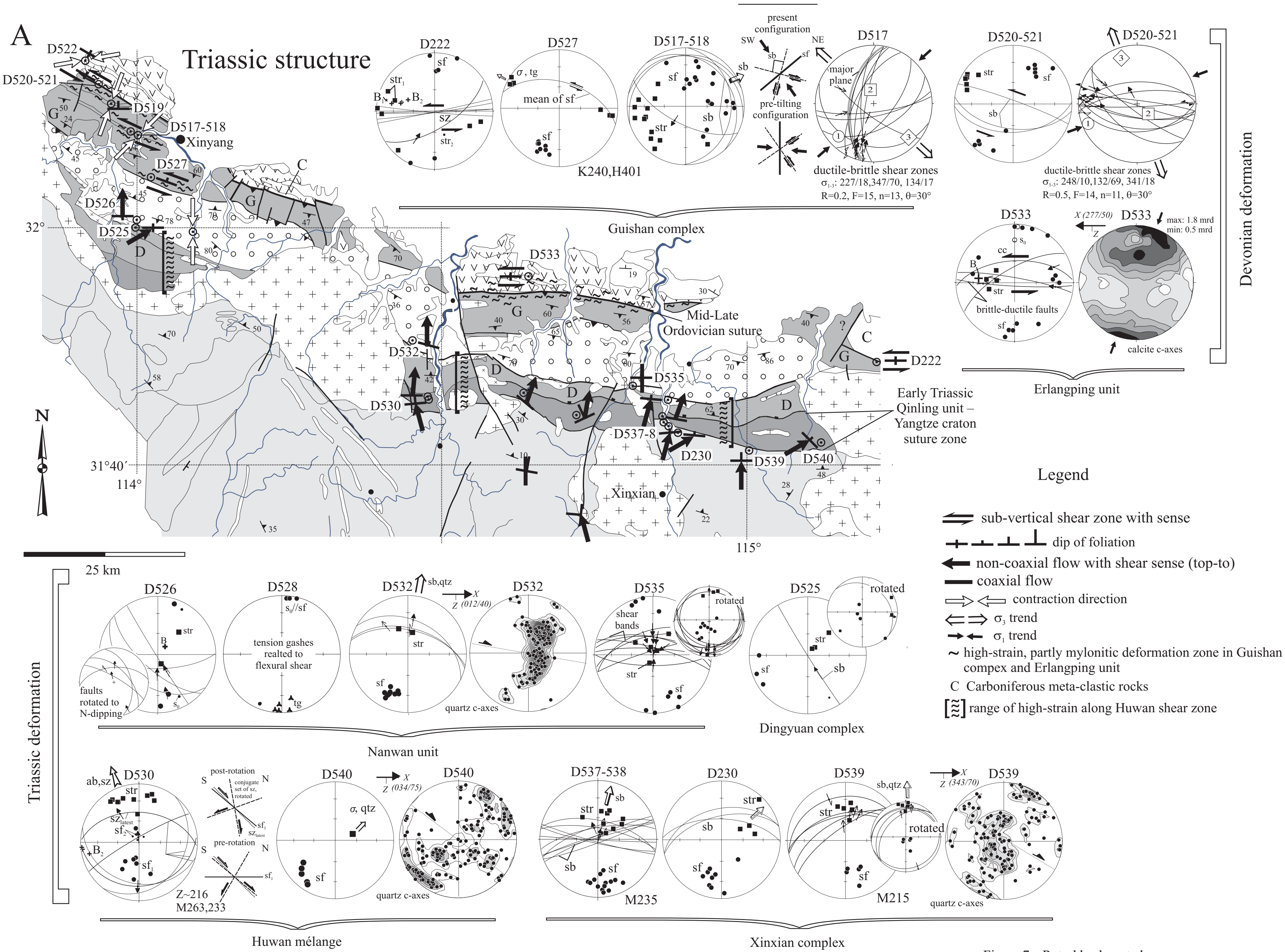

Figure 7a, Ratschbacher et al.

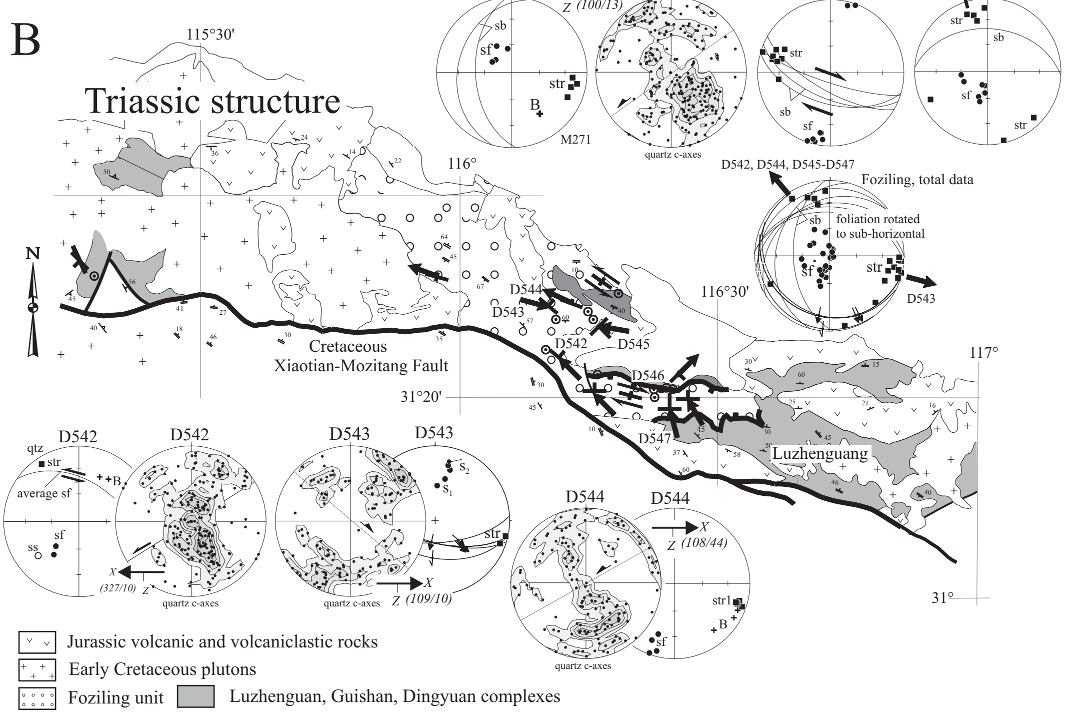

Figure 7b, Ratschbacher et al.

TABLE 1. ^{40}AR/^{39}AR DATA FROM XINXIAN–DABIE

Sample	Rock and Unit	Coordinates	
D222d	meta-volcaniclastic mylonitic gneiss with amphibolite and leucocratic quartz-feldspar layers, Guishan	31°48.45’	115°15.15’
D236	potassium-feldspar vein in a garnet-hornblende-biotite orthogneiss, Xinxian	31°30.09’	114°39.62’
D329b	potassium-feldspar megacrystic quartzofeldspathic gneiss, Hong’an	31°16.0’	114°09.9’
D337a	banded gneiss with mafic layers, Dingyuan	31°45.197’	114°47.934’
D527b	potassium-feldspar augen in mylonitic tourmaline-hornblende gneiss, Guishan	32°03.966’	114°01.873’
D538d	felsic gneiss, northernmost Xinxian	31°43.406’	114°52.374’
D539a	felsic orthogneiss and micaschist, northernmost Xinxian	31°41.346’	115°00.356’
D545c	biotite-bearing, gneissic quartzite (meta-volcanic), Foziling	31°28.975’	116°12.173’

Sample	J	Weight (mg)	Grain Size (µm)	Interpretation
Potassium–feldspar (multi-diffusion domain, qualitative interpretation)				
D222d	0.0040573	2.2	400	rapid cooling at ~100 Ma
D236	0.0042144	1.8	400	slow cooling between 135–110 Ma, rapid cooling 100–105 Ma
D329b	0.0040316	1.5	200	>150 Ma rock, Cretaceous reheating and rapid cooling at ~105 and ~95 Ma
D337a	0.0041142	1.7	400	rapid cooling from 110–125 Ma
D527b	0.008560	8.0	1000	>275 Ma rock, reheating at ~240 Ma

Sample	mineral	J	Weight (mg)	Grain size (µm)	TFA	WMA	isochron	MSWD or Correlation	40/36	% Ar
Muscovite										
D538d	mus	0.008560	4.0	200	234.9±2.5	*234.9±2.5*	230.3±4.4	0.7243	360±104	100
D539a	mus	0.0007004	4.1	400	213.5±0.6	*214.5±0.6*	214.7±0.7	21/1.9	290±6	92
D545c	mus	0.008560	6.1	200	270.8±2.2	*270.7±2.0*	270.5±1.2	0.9964	402±16	92

Italics: preferred age

TABLE 2. SAMPLE LOCATIONS AND APATITE FISSION-TRACK DATING PARAMETERS

sample	Latitude (N)	Longitude (E)	Elevation (m)	grains	N_s	N_i	ρ_d (10^5 cm^{-2})	ϕ (10^{15} cm^{-2})	ζ (a cm^2)	Z (10^8 a)	$P(\chi^2)$	ϕ – age (Ma)	ζ-age (Ma)	Z –age (Ma)
DS43*	31°22.400’	116°11.500’	180	27	276	917	16.4	9.670	369	5.76	20	87.7 ± 6.3	90.2 ± 6.5	86.0 ± 6.4
DS58*	31°14.340’	116°20.390’	190	20	1912	6671	16.4	9.730	369	5.78	2	83.6 ± 3.0	85.8 ± 3.1	81.9 ± 3.0
DS72*	31°07.480’	116°31.520’	400	26	664	2885	16.5	9.670	369	5.79	26	67.2 ± 3.2	69.6 ± 3.4	66.3 ± 3.4
D516*	31°43.140'	116°30.584'	100	14	954	714	3.87	2.580	369	1.53	0	116.0 ± 6.7	105 ± 6	113 ± 6.5
D517	32°07.455'	114°00.285'	200	11	846	439	3.87	2.581	369	1.53	0	128 ± 14	117 ± 13	124 ± 13
D519	32°10.289'	113°57.335'	100	17	1580	2580	3.87	2.580	369	1.53	6	47.7 ± 1.8	43.6 ± 1.8	46.7 ± 2.3
D523	31°54.94-'	113°57.702'	100	7	150	126	3.87	2.579	369	1.53	43	92.5 ± 11.0	84.4 ± 10	90.4 ± 11
D524	31°53.823'	113°57.925'	100	23	1090	2106	3.87	2.578	369	1.53	0	48.2 ± 5.5	44.0 ± 5.0	47.1 ± 5.4
D527	32°03.966'	114°01.873'	80	25	1759	936	3.87	2.575	369	1.53	40	145.0 ± 6.6	133 ± 6.3	142 ± 7.8
D532	31°50.148'	114°27.146'	90	20	1535	1329	3.87	2.574	369	1.53	21	89.6 ± 3.8	81.9 ± 3.7	87.8 ± 4.6
D533	31°56.971'	114°38.547'	150	10	757	993	3.87	2.573	369	1.53	3	61.3 ± 4.6	56.1 ± 4.3	60.1 ± 4.6
D535	31°46.833'	114°48.748'	90	9	503	382	3.87	2.572	369	1.53	23	102.0 ± 7.2	93.3 ± 6.7	100 ± 7.7
D536	31°44.850'	114°48.864'	100	25	1262	1499	3.87	2.571	369	1.53	37	65.3 ± 2.8	59.8 ± 2.7	64.1 ± 3.4
D538	31°43.200'	114°52.473'	90	56	947	1066	3.87	2.540	369	1.53	37	68.1 ± 3.3	63.1 ± 5.1	67.6 ± 3.9
D539	31°41.346'	115°00.356'	100	14	153	210	3.87	2.530	369	1.53	14	55.7 ± 6.0	51.8 ± 5.7	55.5 ± 6.3
D540	31°42.134'	115°07.478'	260	20	286	520	3.87	2.519	369	1.53	65	41.9 ± 3.2	39.2 ± 7.8	41.9 ± 3.5
D543*	31°27.736'	116°10.498'	320	40	3204	3337	3.87	2.510	369	1.53	13	72.7 ± 2.3	68.2 ± 2.4	73.0 ± 3.3
D545*	31°28.975'	116°12.173'	280	7	343	402	3.87	2.490	369	1.53	78	64.1 ± 4.9	60.6 ± 4.7	64.9 ± 5.4
D546	31°21.877'	116°22.297'	100	10	140	247	6.21	4.009	341	2.14	12	67.1 ± 7.2	59.7 ± 6.4	60.4 ± 6.8
D549	31°12.511'	116°22.739'	190	23	565	1197	6.21	4.001	341	2.14	80	55.8 ± 3.1	53.9 ± 3.0	50.3 ± 3.3
D552	31°04.699'	116°21.012	780	20	1121	1805	6.21	3.994	341	2.14	47	73.2 ± 3.1	65.4 ± 2.7	66.1 ± 3.7
D98-17*	31°10.299'	116°32.279'	–	34	4271	4844	3.87	2.410	369	1.53	0	60.2 ± 1.5	59.0 ± 1.3	63.1± 1.4
CN104	31°24.370'	114°40.158'	125	23	401	448	6.21	3.899	341	2.14	98	103.0 ± 7.4	94.1 ± 6.7	95.1 ± 7.6
CN106	31°19.737'	114°22.615'	148	30	752	1483	6.21	3,874	341	2.14	1	61.5 ± 3.9	56.6 ± 3.6	57.2 ± 3.6
CN110	32°04.573'	113°32.067'	325	14	757	2141	6.21	3.899	341	2.14	0	40.3 ± 3.1	37.3 ± 2..9	37.7 ± 2.9
CN111a	32°08.512'	113°35.225'	295	23	1255	2604	6.21	3.852	341	2.14	43	54.9 ± 2.2	50.8 ± 1.9	51.4 ± 2.7
CN112	32°20.518'	113°36.500'	75	26	2125	3907	6.21	3.806	341	2.14	0	66.6 ± 4.0	62.5 ± 3.7	63.1 ± 3.8
CN113	32°21.112'	113°25.868'	152	30	710	1229	6.21	3.776	341	2.14	84	64.4 ± 3.3	60.9 ± 3.0	61.5 ± 3.8
CN136	31°15.927'	113°53.312'	45	19	505	374	6.21	3.547	341	2.14	84	141 ± 10	141 ± 10	143 ± 11

*data published in Grimmer et al. (2002); N_s: number of spontaneous tracks; N_i: number of induced tracks; ρ_d: track density on dosimeter; ϕ: neutron flux density; Z: Z-calibration factor; ζ: ζ_{CN5} -calibration factor; $P(\chi)^2$ is the probability of obtaining χ^2 value for ν degrees of freedom (where ν = number of grains - 1).

TABLE 3: CONFINED TRACK-LENGTH PARAMETERS IN APATITE

sample	N	MTL [μm]	Std.
D519	106	13.0	1.6
D524	33	13.0	1.4
D527	106	12.8	1.3
D532	108	11.9	1.9
D533	12	11.8	2.0
D536	70	12.7	1.6
D538	15	13.0	1.9
D540	10	10.9	2.5
D72	40	13.4	1.2
D98-17	105	12.0	1.6

N: number of tracks; MTL: mean track length;
Std.: standard deviation.

TABLE 4. SAMPLE LOCATIONS AND SPHENE FISSION-TRACK DATING PARAMETERS

sample	Latitude (N)	Longitude (E)	grain	N_s	N_i	ρ_d (10^5cm^{-2})	ζ (a cm^2)	$P(\chi)^2$ %	ζ-age (Ma)
CN111b	32°08.307'	113°35.135'	20	1089	2089	7.66	423	67	83.9 ± 6.6
CN113	32°21.067'	113°25.521'	10	1263	2087	7.66	423	0	97.1 ± 6.5
DS58	31°14.340’	116°20.390’	8	1312	907	4.27	423	15	129.3 ± 9.7
DS72	31°07.480’	116°31.520’	18	1687	1340	4.27	423	77	112.7 ± 8.0
D98-17	31°10.299'	116°32.279'	11	1955	2381	7.66	423	85	131.7 ± 9.2
D536	31°44.850'	114°48.864'	20	1158	974	4.27	423	79	106.5 ± 8.0

N_s: number of spontaneous tracks; N_i: number of induced tracks; ρ_d: track density on dosimeter; ϕ: neutron flux density; Z: Z-calibration factor; ζ: ζ_{CN5} -calibration factor; $P(\chi)^2$ is the probability of obtaining χ^2 value for ν degrees of freedom (where ν = number of grains - 1).

TABLE 5. NEW PETROLOGY FROM XINXIAN

Sample/Station	Rock Type	Unit	Mineral Assemblage	Pressure–Temperature Estimate
98196/D539	eclogite	Xinxian complex	Grt - Omp - Phg - Czo - Qtz ± Rt, Ap	530°C/2.21 GPa
98185/D530	eclogite	Huwan mélange (Xiongdian)	Grt - Omp - Phg - Czo - Qtz ± Rt, Ap	536°C/2.01 GPa
D530c/D530	eclogite	Huwan mélange (Xiongdian)	Grt - Omp - Phg - Czo - Bar - Qtz ± Rt, Ap	595°C/2.06 GPa
98181/D530	garnet amphibolite	Huwan mélange (Xiongdian))	Grt - Mg-Hbl - Pl (An_{10-12}) - Phg - Czo - Qtz ± Rt, Ilm, Ap	560°C/1.1 GPa
98182/D530	garnet-mica schist	Huwan mélange (Xiongdian)	Grt - Phg - Czo - Qtz - Ab ± Rt, Spn	600°C/1.8 GPa
D525a/D525	greenschist	Dingyuan complex	Act/Mg-Hbl - Ep - Chl - Ab - Phg - Qtz ± Cc, Spn, Zrn, Ap	core: 480°C/0.71 GPa; rim: 420°C/0.43 GPa
D527d/D527	amphibolite	Guishan complex	Ed/Prg - Pl (An_{34-41}) - Qtz - Bt ± Ilm, Ap	740°C/0.9 GPa; HP/LT overprint: 250-300°C/0.4-0.65 GPa
D527e/D527	amphibolite	Guishan complex	Mg-Hs - Pl (An_{33-37}) - Qtz - Bt ± Ilm, Ap	680°C/1.1 GPa
D522a/D527	amphibolite	Erlangping unit	Act/Mg-Hbl - Ep - Chl - Ab - Phg ± Qtz, Ilm	core: 350°C/1 GPa; rim: 555°C/0.63 GPa

See Table 2 for locations (latitude, longitude), except for D530, 31°45.151’, 114°28.340’; D525, 32°00.052’, 113°59.243’. Mineral abbreviations follow Kretz (1983), except for Bar=barroisite, Phg=phengite.